The Astrophysical Journal, 625:474–495, 2005 May 20

SHOCK GEOMETRY, SEED POPULATIONS, AND THE ORIGIN OF VARIABLE ELEMENTAL COMPOSITION AT HIGH ENERGIES IN LARGE GRADUAL SOLAR PARTICLE EVENTS

A. J. Tylka,[1] C. M. S. Cohen,[2] W. F. Dietrich,[3] M. A. Lee,[4] C. G. Maclennan,[5]
R. A. Mewaldt,[2] C. K. Ng,[6,7] and D. V. Reames[6]
Received 2004 February 16; accepted 2005 February 3

ABSTRACT

Above a few tens of MeV per nucleon, large, gradual solar energetic particle (SEP) events are highly variable in their spectral characteristics and elemental composition. The origin of this variability has been a matter of intense and ongoing debate. In this paper, we propose that this variability arises from the interplay of two factors—shock geometry and a compound seed population, typically comprising both solar-wind and flare suprathermals. Whereas quasi-parallel shocks generally draw their seeds from solar-wind suprathermals, quasi-perpendicular shocks—by requiring a higher initial speed for effective injection—preferentially accelerate seed particles from flares. Solar-wind and flare seed particles have distinctive compositional characteristics, which are then reflected in the accelerated particles. We first examine our hypothesis in the context of particles locally accelerated near 1 AU by traveling interplanetary shocks. We illustrate the implications of our hypothesis for SEPs with two very large events, 2002 April 21 and 2002 August 24. These two events arise from very similar solar progenitors but nevertheless epitomize extremes in high-energy SEP variability. We then test our hypothesis with correlation studies based on observations of 43 large SEP events in 1997–2003 by the *Advanced Composition Explorer*, *Wind*, the *Interplanetary Monitoring Platform 8*, and *GOES*. We consider correlations among high-energy Fe/O, event size, spectral characteristics, the presence of GeV protons, and event duration at high energies. The observed correlations are all qualitatively consistent with our hypothesis. Although these correlation studies cannot be construed as proof of our hypothesis, they certainly confirm its viability. We also examine the alternative hypothesis in which a direct flare component—rather than flare particles subsequently processed through a shock—dominates at high energies. This alternative would produce compositional characteristics similar to those of our hypothesis. However, the observed longitude distribution of the enhanced Fe/O events, their spectral characteristics, and recent timing studies all pose serious challenges for a direct flare component. We also comment on measurements of the mean ionic charge state of Fe at high energies. We conclude that shock geometry and seed population potentially provide a framework for understanding the overall high-energy variability in large SEP events. We suggest additional studies for testing this hypothesis.

Subject headings: acceleration of particles — shock waves — Sun: coronal mass ejections (CMEs) — Sun: flares — Sun: particle emission

1. INTRODUCTION

Large solar energetic particle (SEP) events, in which the primary accelerators are shocks driven by fast coronal mass ejections (CMEs), are productive opportunities for refining our understanding of shock acceleration (Reames 1999; Lee 2000, 2005; Zank et al. 2000; Rice et al. 2003; Cliver et al. 2004) and particle transport (Ng et al. 1999, 2003; Li et al. 2003). Heavy ions (with atomic number $Z \geq 2$) are especially powerful probes in this regard. Isotopic ratios (i.e., ^{3}He/^{4}He) and elemental ratios (especially Fe/C or Fe/O, when combined with ionic charge state measurements) are signatures of specific seed populations. Moreover, because the minor ions (with $Z > 2$) are test particles with a range of charge-to-mass (Q/A) ratios, they potentially provide a means of untangling the various velocity- and rigidity-dependent effects that govern injection, acceleration, and transport.

Figure 1 illustrates two extremes in the variability of elemental composition among large SEP events. In order of increasing energy, the measurements come from the Ultra Low Energy Isotope Spectrometer (ULEIS; Mason et al. 1998) on the *Advanced Composition Explorer* (*ACE*), the Electron, Proton, and Alpha Monitor (EPAM; Gold et al. 1998) on *ACE*, the Low Energy Matrix Telescope (LEMT) in the Energetic Particle Acceleration, Composition, and Transport (EPACT) experiment (von Rosenvinge et al. 1995) on *Wind*, and the Solar Isotope Spectrometer (SIS; Stone et al. 1998a) on *ACE*. The figure shows the event-integrated Fe/C ratio as a function of energy for the events of 2002 April 21 and 2002 August 24. These two events are, respectively, the largest SEP event in 2002 (in terms of total proton fluence above 30 MeV) and the only ground-level event (GLE) in 2002. From $\sim$0.5 to $\sim$10 MeV nucleon^{-1}, the Fe/C ratios are nearly identical in the two events. But at higher energies the two events diverge, so that the Fe/C ratio at the highest measured energy ($\sim$60 MeV nucleon^{-1}) differs by more than 2 orders of magnitude. The energy dependence of Fe/C reflects, of course, spectral differences between the two species. In the April event,

[1] E. O. Hulburt Center for Space Research, Naval Research Laboratory, Code 7652, Washington, DC 20375; allan.tylka@nrl.navy.mil.
[2] California Institute of Technology, MC 220-47, Pasadena, CA 91125; cohen@srl.caltech.edu, rmewaldt@srl.caltech.edu.
[3] Laboratory for Astrophysics and Space Research, Enrico Fermi Institute, University of Chicago, 5640 Ellis Avenue, Chicago, IL 60637; dietrich@odysseus.uchicago.edu.
[4] Space Science Center and Institute for the Study of Earth, Oceans, and Space, University of New Hampshire, Durham, NH 03824-3525; marty.lee@unh.edu.
[5] Bell Laboratories, Lucent Technologies, 600 Mountain Avenue, Murray Hill, NJ 07974; cgm@physics.bell-labs.com.
[6] NASA Goddard Space Flight Center, Code 661, Greenbelt, MD 20771; reames@milkyway.gsfc.nasa.gov.
[7] Department of Astronomy, University of Maryland, College Park, MD 20742; cheeng@lheapop.gsfc.nasa.gov.

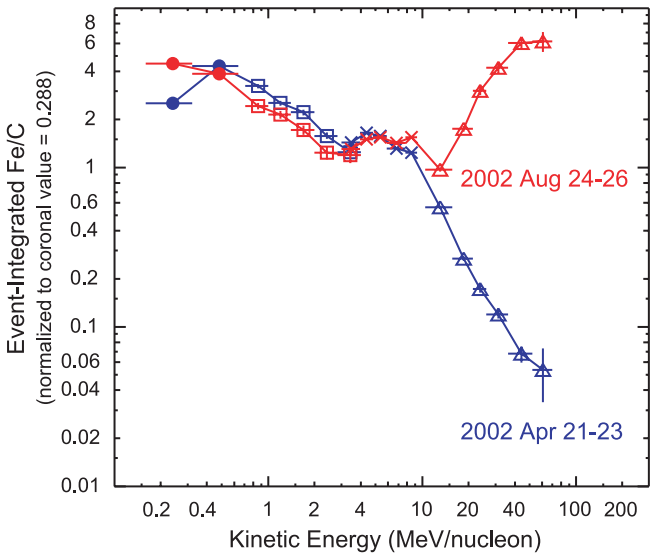

FIG. 1.—Event-integrated Fe/C (normalized to the nominal coronal value 0.288; Reames 1995) vs. energy for the SEP events of 2002 April 21 (*blue*) and 2002 August 24 (*red*). Data come from ULEIS (Mason et al. 1998; *filled circles*) on *ACE*, EPAM (Gold et al. 1998; *open squares*) on *ACE*, LEMT in the EPACT experiment (von Rosenvinge et al. 1995; *crosses*) on *Wind*, and SIS (Stone et al. 1998a; *open triangles*) on *ACE*.

Fe has a softer spectrum than C at higher energies; in the August event, it is harder. The large-fluence event is Fe-poor at high energies, while the GLE is Fe-rich.

About one-third of the large SEP events observed by *ACE* and *Wind* in solar cycle 23 exhibit significant energy dependence in Fe/C, similar to those in Figure 1. *Interplanetary Monitoring Platform 8* (*IMP8*) also showed comparable variability (albeit with less statistical precision) in previous solar cycles (Tylka & Dietrich 1999; Mazur et al. 1992). However, this difference is especially noteworthy for the two particular events in Figure 1: the solar progenitors of these events are fortuitously similar. Both events were produced by wide CMEs, in which the speeds[8] were $\sim$2400 km s^{-1} for the April event and $\sim$1900 km s^{-1} for the August event. Of the nearly 7000 CMEs observed by the *Solar and Heliospheric Observatory* (*SOHO*) in 1997–2002, these two rank as the 6th and 18th fastest, respectively (S. Yashiro 2004, private communication); both were easily capable of driving a shock throughout most, if not all, of the corona. Transit times to Earth for the associated shocks were 51 and 58 hr, respectively. The associated flares for the two events were also nearly identical in terms of their sizes and solar locations (X1.5/1F at S14°, W84°; and X3.1/1F at S02°, W81°, respectively).[9] Thus, the difference in Figure 1 cannot be blithely ascribed to factors such as CME speed and source location, which are generally important for SEP variability. Instead, Figure 1 challenges us to look for a more subtle driver behind the high-energy behavior.

[8] CME parameters were provided by http://cdaw.gsfc.nasa.gov/CME_list. Information on flares was taken from http://www.ngdc.noaa.gov/stp/SOLAR/sgdintro.html.

[9] In the nominal Parker-spiral magnetic field, direct connection to these flare longitudes would require solar-wind speeds of 273–283 km s^{-1}. However, the solar-wind speed measured on *Wind* in the first 12 hr of the 2002 April 21 event varied between 452 and 504 km s^{-1}, corresponding to connection longitudes of W46°–W51°. In the first 12 hr of the 2002 August 24 event, the solar-wind speed varied between 345 and 436 km s^{-1}, corresponding to connection longitudes at W52°–W66°. Thus, there is no a priori reason to expect direct connection to the flare site in either event.

Events with highly suppressed Fe/C at high energies are easy to understand in terms of a shock operating on a seed population dominated by solar-wind suprathermals. From very general considerations, a common *Ansatz* for the differential energy spectrum of shock-accelerated particles is the functional form $F(E) \sim E^{-\gamma} \exp(-E/E_0)$ (Ellison & Ramaty 1985; Jones & Ellison 1991). In the simplest interpretation (which neglects many factors, including nonequilibrium conditions and spectral distortions due to transport), the power-law index γ is determined by the shock compression ratio. The *e*-folding energy E_0, on the other hand, reflects the diffusion coefficient that controls escape from the near-shock region. For some events (such as 2002 April 21) this *e*-folding energy has a relatively low value, and we clearly see the exponential rollover in ion spectra below $\sim$100 MeV nucleon^{-1}. As we argue below, these are likely to be quasi-parallel shocks—at least while near the Sun, where shocks are generally most prolific at accelerating particles to high energies. Ellison & Ramaty (1985) also suggested that E_0 scales with the ion's Q/A value when the near-shock scattering mean free path is directly proportional to rigidity. Physically, this scaling reflects the fact that at any given momentum, particles with higher A/Q are more likely to escape the shock region and thereby lose the opportunity to be promoted to even higher energies. Thus, if a shock operates on a seed population dominated by solar-wind–like suprathermals (with C having $Q/A \sim 0.5$ while $Q/A \sim 0.2$ for Fe), then Fe has a smaller *e*-folding energy E_0. The Fe spectrum therefore rolls over more steeply than the C spectrum, leading to highly suppressed Fe/C at high energies. In fact, this behavior has been exploited to determine ionic charge states for various elements in the 2002 April 21 event and in other events with similar characteristics (Tylka et al. 2000, 2001; Tylka 2001). The charge states deduced from these spectral comparisons are in good agreement with directly measured values from the *Solar, Anomalous, and Magnetospheric Particle Explorer* (*SAMPEX*) and *ACE* in these events.

But understanding how shock acceleration can produce events like 2002 August 24, in which Fe/C increases with energy and attains values $\gtrsim$5 times that of the corona, has proven to be more elusive (Mason et al. 1999b; Tylka et al. 2002; Cane et al. 2003; Cohen et al. 2003). These events also tend to have enhanced ^{3}He/^{4}He above 7 MeV nucleon^{-1} (Cohen et al. 1999; Wiedenbeck et al. 2000; Cane et al. 2003; Torsti et al. 2003). For a few such events there are direct (Leske et al. 2001; Labrador et al. 2003) and indirect (Dietrich & Tylka 2003) measurements of the mean ionic charge of Fe ($\langle Q_{\rm Fe}\rangle$) above $\sim$30 MeV nucleon^{-1}. In these events, $\langle Q_{\rm Fe}\rangle \sim 20$. As a result, Fe and C have not too dissimilar Q/A values, and it is difficult to ascribe the Fe/C enhancement to transport or acceleration effects. Consequently, the enhanced Fe/C must be a characteristic of the seed population from which the highest energy ions are drawn.[10]

As illustrated schematically in Figure 2, the seed population for SEPs likely comprises at least two components: the ubiquitous suprathermal tail from the solar wind (Gloeckler et al. 2000) and suprathermals from flare activity (Mason et al. 1999a; Tylka et al. 2001). Among the distinguishing characteristics of these flare suprathermals are elevated Fe/C (and Fe/O) $\sim$10 times the average coronal and solar-wind values, large enhancements in trans-Fe ions (Reames 2000; Reames & Ng 2004; Mason et al. 2004), Fe ions with $\langle Q_{\rm Fe}\rangle > 16$ (Luhn et al. 1987), and ^{3}He/^{4}He

[10] It has also been suggested that the high-charge Fe ions are generated by stripping during acceleration in high-density regions of the corona (Reames et al. 1999; Barghouty & Mewaldt 1999, 2000). But it is not clear why this process should also lead to enhanced Fe/C.

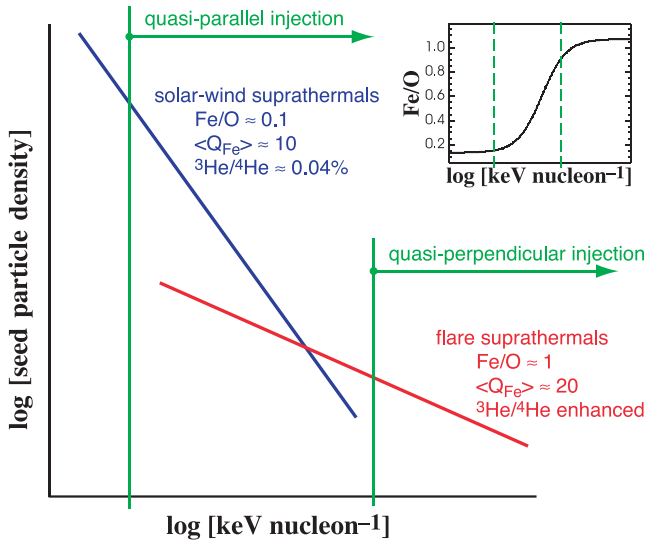

FIG. 2.—Schematic representation of the suprathermal seed population for shock-accelerated solar energetic particles, comprising both solar-wind and flare-accelerated ions. The flare suprathermals are more likely to be apparent in quasi-perpendicular shocks, for which the injection threshold is higher. The inset (*upper right*) shows how the Fe/O ratio in the seed population changes with energy. As the geometry evolves as the shock moves out from the Sun (generally, from quasi-perpendicular toward quasi-parallel), the nature of the accessible seed population would also change.

significantly enhanced above the average solar-wind value of $0.041\% \pm 0.003\%$ (Gloeckler & Geiss 1998). A recent survey (Wiedenbeck et al. 2003) has shown that particles from flare activity, as evidenced by energetic ^{3}He above 200 keV nucleon^{-1}, are present in the interplanetary medium at 1 AU at least 60% of the time during solar maximum. (See also Richardson et al. 1990 and Laivola et al. 2003.) Mewaldt et al. (2003a) have also estimated that remnant flare suprathermals are sufficiently numerous that they alone could provide the seed particles for all of the observed SEP iron[11] above 1 MeV nucleon^{-1}. Although the relative strength of these two components can vary from event to event, their combined presence naturally leads to an energy-dependent composition in the seed population, with both the relative abundance of Fe and $\langle Q_{\rm Fe}\rangle$ increasing with particle speed.

Generally, one would expect solar-wind suprathermals to vastly outnumber flare suprathermals. However, a substantial body of theoretical work suggests that the minimum particle speed needed to participate in shock acceleration should be higher for quasi-perpendicular shocks, either for simple kinematic reasons (Forman & Webb 1985) or because the acceleration efficiency is higher for faster seed particles (Jokipii 1987; Webb et al. 1995; Zank et al. 2004). The kinematic considerations (Forman & Webb 1985) are based on the notion of "catching-up" to the shock from the downstream region. However, more careful analysis shows that the required conditions for acceleration at a quasi-perpendicular shock are more complicated than that; they depend instead upon both the nature of the particle's interaction with the shock and the details of the scattering conditions. Jokipii (1987) envisioned acceleration at a perpendicular shock as the particle drifting along the shock front, gaining energy while its gyroradius is engulfed by the shock. Maintaining particle isotropy, as required for efficient acceleration, then implies that the particle must be scattered during this engulfment. From these considerations, Jokipii (1987) concluded that the initial particle speed for acceleration at a quasi-perpendicular shock must be much higher than the shock speed, whereas injection at a quasi-parallel shock can occur when the initial particle speed is only slightly larger than that of the shock. Moreover, as numerous authors have pointed out, cross-field diffusion, rather than particle speed, plays the key role in returning the particle to the upstream region at a perpendicular shock (Jokipii 1987; Jones et al. 1993; Achterberg & Ball 1994; Webb et al. 1995). For example, Webb et al. (1995) showed that, all other things being equal, the minimum injection speed in a perpendicular shock is larger than that in a parallel shock by a factor of $(K_\parallel/K_\perp)^{1/2}$, where $K_\parallel$ and $K_\perp$ are the diffusion coefficients parallel and perpendicular to the upstream magnetic field, respectively. If $K_\perp/K_\parallel \sim 1\%$ (Giacalone & Jokipii 1999; Zank et al. 2004; Bieber et al. 2004), then the minimum injection speed at the perpendicular shock would be higher by about a factor of ten.[12]

Thus, as also illustrated schematically in Figure 2, flare suprathermals are more likely to dominate over solar-wind suprathermals as the seed particles in quasi-perpendicular shocks. However, the shock geometry generally evolves as the shock moves out from the Sun, usually from quasi-perpendicular toward quasi-parallel. The nature of the accessible seed population would also change during this evolution. At the same time, as the shock angle decreases, the spectra soften at high energies. The net effect of this evolution is to allow the unique compositional characteristics of flare suprathermals to be reflected preferentially among the higher energy particles.

In this paper we therefore suggest that events like 2002 August 24 involve quasi-perpendicular shocks, operating on a seed population containing suprathermal ions from flare activity. These flare suprathermals could be remnants from earlier flare activity (Mason et al. 1999a; Tylka et al. 2001) or come from the associated flare, if open field lines connect the flare site to the shock front (Reames 2002). The acceleration process in quasi-perpendicular shocks is rapid, giving them a distinct advantage in producing high-energy particles (Jokipii 1987; Decker 1988; Ostrowski 1988; Giacalone et al. 1994; Webb et al. 1995; Zank et al. 2004). Rapid acceleration is particularly critical in the case

[11] In fact, in the analysis below, we suggest that flare suprathermals generally provide seeds for energetic particles above ~10 MeV nucleon^{-1}, and that they are not important at all in some of the largest fluence events, such as 2002 April 21. Consequently, only a few percent of the remnant flare suprathermals would be necessary to account for the observed high-energy enhancements in SEP Fe. The enhanced Fe below ~1 MeV nucleon^{-1} in Fig. 1 is not the focus of this paper. However, we suggest in passing that this enhancement may be a transport-induced distortion (due to iron's relatively low Q/A), rather than an attribute of the seed population. SEPICA (Möbius et al. 1998) on *ACE* has presented preliminary measurements for seven of the SEP events in this study at http://cdaw.gsfc.nasa.gov/LWS/data. In these events, the mean charge states for iron at 0.23–0.33 MeV nucleon^{-1} are $\langle Q_{\rm Fe}\rangle \sim 10$–13; the mean charge states for oxygen at 0.50–0.63 MeV nucleon^{-1} are $Q_{\rm O} \sim 6$–7. These charge states are characteristic of solar-wind ions, not flare-accelerated ions. *ACE* ULEIS has also reported event-integrated Fe/O at 0.16–0.32 MeV nucleon^{-1} for six of these events. The values are enhanced at ~2–7 times the nominal solar-wind/coronal value.

[12] Fundamental observational facts, such as the organization of the shapes of SEP time-intensity profiles by longitude (Cane et al. 1988; Reames et al. 1996) and the existence of flux dropouts in impulsive events (Mazur et al. 2000), argue that $K_\perp/K_\parallel \ll 1$, at least during the interplanetary transport of SEPs. We note, however, the appropriate value for $K_\perp/K_\parallel$ in the turbulence of the shock region is not well understood. Also, Giacalone (2005) has warned that the shock geometry's effect on the injection threshold may be weakened in cases where the large-scale magnetic field fluctuations are strong. Of course, these conditions are poorly known in active regions of the corona. We may therefore look upon these studies as an opportunity to pin down those conditions, using the remote sensing capabilities provided by the high-energy SEPs.

of high-energy SEPs, since the maximum energy attainable by the CME-driven shock generally decreases quickly as the shock moves outward from the Sun (Lee 1997; Ryan et al. 2000; Zank et al. 2000). For this reason, quasi-perpendicular shocks are more likely to produce GLEs.

The outline of this paper is as follows. In § 2 we examine energetic particles produced by traveling interplanetary shocks near 1 AU, focusing on events that exhibit the same extreme range of energy dependence in Fe/O as the SEP events of Figure 1. In § 3 we show how other characteristics of the large SEP events (including fluences, spectral characteristics, the presence of GeV particles, and durations at high energies) are consistent with our hypothesis. In § 4 we comment on an alternative hypothesis in which a *direct* flare component—rather than flare particles subsequently processed through a shock—dominate at high energies. In § 5 we summarize our results, note some particular challenges for our hypothesis, and discuss future studies that may be able to test it.

2. TRAVELING INTERPLANETARY SHOCK EVENTS NEAR 1 AU

We first employ observations of traveling interplanetary shocks near 1 AU (hereafter referred to as IPS events) to examine our hypothesis about the roles of shock geometry and seed populations. For these IPS events we have a local measurement of θ_{Bn}, the angle between the upstream magnetic field vector $\boldsymbol{B}$ and the shock normal $\boldsymbol{n}$. We also have measurements of the ^{3}He/^{4}He ratio in the accelerated particles, which generally provides an indicator of flare remnants in the seed population. We note, however, that θ_{Bn} and ^{3}He/^{4}He are only imperfect proxies for the factors whose impact we wish to assess. Energetic particle measurements (especially for heavy ions) necessarily average over an extended time period and combine particles produced at various locations on the shock front. At best, a single θ_{Bn} measurement is representative of the changing shock geometry during this time interval. Similarly, since enhancements of ^{3}He/^{4}He and Fe/O in flares are produced by distinct mechanisms, one can be present in the seed population without the other.

Desai et al. (2003) published a list of 72 IPS events observed by *ACE* ULEIS in 1997–2002. To identify events in which ions were indeed accelerated near 1 AU, they required no velocity dispersion among the onset times of Fe ions at 0.3–3.0 MeV nucleon^{-1}. Desai et al. (2004) also provided the θ_{Bn} values for these events. This event list was the starting point for our analysis. We used data from *Wind* LEMT (whose geometry factor is ~50 times larger than that of *ACE* ULEIS) to extend the Desai et al. (2003) measurements beyond ~2 MeV nucleon^{-1}, thereby better defining the energy dependence. For a few events, *ACE* SIS also saw a shock-related increase from which we were able to derive Fe/O at 10–15 MeV nucleon^{-1}. (See also Desai et al. 2004.)

The shock angle θ_{Bn} generally changes as the shock moves through the interplanetary medium. As already noted, a particular concern in studying IPS events is how well the locally measured θ_{Bn} actually reflects conditions at the location where the observed energetic particles were accelerated. To minimize these concerns, we have shortened the integration intervals as much as the shape of the time profiles would justify. Our integration intervals were generally shorter than those of Desai et al. (2003), who were trying to maximize ion statistics. For example, for the 23 IPS events discussed below, the Desai et al. integration intervals ranged from 9 to 71 hr in duration, with an average of 32 hr; in our analysis, the integration intervals in these same events ranged from 2 to 36 hr, with an average of 15 hr.

In order to investigate the extreme behavior analogous to that in Figure 1, we selected only those IPS events in which Fe/O showed a strong energy dependence, starting from near-coronal values and changing by roughly an order of magnitude or more, either increasing or decreasing.[13] Twenty-three events satisfied these criteria. Eighteen of the events have Fe/O falling with energy, while five show Fe/O clearly rising with energy.[14] The events with increasing Fe/O are the same ones identified by Desai et al. (2004). *Wind* LEMT confirms that Fe/O is enhanced in these events, although with large statistical uncertainties and generally not as strongly as indicated by the *ACE* ULEIS measurements above ~1 MeV nucleon^{-1}. This difference may reflect systematic instrumental effects that are not yet understood.

Figure 3 shows two different views of Fe/O versus energy for the selected events. In the left panel, the Fe/O values are normalized to the nominal coronal value; in the right panel, each event is normalized to its observed Fe/O value at 0.08–0.16 MeV nucleon^{-1}. The colors in the left and right panels of Figure 3 indicate, respectively, the values of ^{3}He/^{4}He and θ_{Bn} from Desai et al. (2003, 2004). From these colors one sees that events with rising Fe/O are preferentially associated with large ^{3}He/^{4}He and θ_{Bn}. On the other hand, events with falling Fe/O generally have smaller ^{3}He/^{4}He and are associated with a full range of θ_{Bn} values. Moreover, the distribution of colors in the right panel hints that among events with falling Fe/O, Fe/O tends to fall more steeply among those with smaller values of θ_{Bn}.

At ~100 keV nucleon^{-1}, Fe/O in these IPS events varies by about a factor of 5. But at ~2 MeV nucleon^{-1}, the variation spans 2 orders of magnitude. Thus, IPS events exhibit the same extreme morphologies as the SEP events in Figure 1. This fact alone suggests that the variability originates in the details of shock acceleration, and not in two distinct acceleration mechanisms. However, the behavior is manifested at lower energies in the IPS events, consistent with the decrease in maximum attainable energy as the CME-driven shock moves outward from the Sun.

In Figure 4 we plot Fe/O versus θ_{Bn}. Each event is represented by Fe/O at 2.5–5.0 MeV nucleon^{-1} from the left panel of Figure 3, except for one event, in which 1.3–1.8 MeV nucleon^{-1} is the highest energy at which a measurement is available. The events in Figure 4 with normalized Fe/O > 1 are those in which Fe/O rises with energy; the events with normalized Fe/O < 1 are those in which Fe/O falls with energy. The colors and shapes of the symbols represent the measured ^{3}He/^{4}He in the IPS event, as explained in the figure caption.

According to Jokipii (1987) and Webb et al. (1995), the advantages of quasi-perpendicular geometry become significant for θ_{Bn} exceeding 60° or 70°, where the particles' rate of energy gain starts to rise sharply with increasing θ_{Bn}. As marked in

[13] We used Fe/C in Fig. 1 because these two abundant minor ions have maximally different Q/A values. Here we use Fe/O, instead of Fe/C, since the oxygen spectrum is generally better measured than the carbon spectrum. The O/C ratio varies relatively little, either event-to-event or with energy within an event, so that Fe/O and Fe/C (normalized to their coronal values) can be used interchangeably in our discussions.

[14] The five events with rising Fe/O are numbers 19, 25, 26, 29, and 37 from the Desai et al. (2003) event list. Desai et al. (2004) also identified a sixth event (number 2 from their list), in which Fe/O increased by a factor of ~3 between 0.1 and 1.0 MeV nucleon^{-1}. At ~1.0 MeV nucleon^{-1} Fe/O in this event was only 2.0 ± 0.6 times the nominal value (M. Desai 2004, private communication) and hence the event was not included in our sample. The 18 events with falling Fe/O are numbers 5, 11, 13, 20, 21, 23, 24, 35, 36, 39, 48, 58, 60, 64, 66, 67, 68, and 69 from the Desai et al. (2003) list. Another event (number 50) also passed our event selection criteria but was subsequently omitted from this study because *ACE* ULEIS was partially saturated for ~10 hr around the time of the shock arrival.

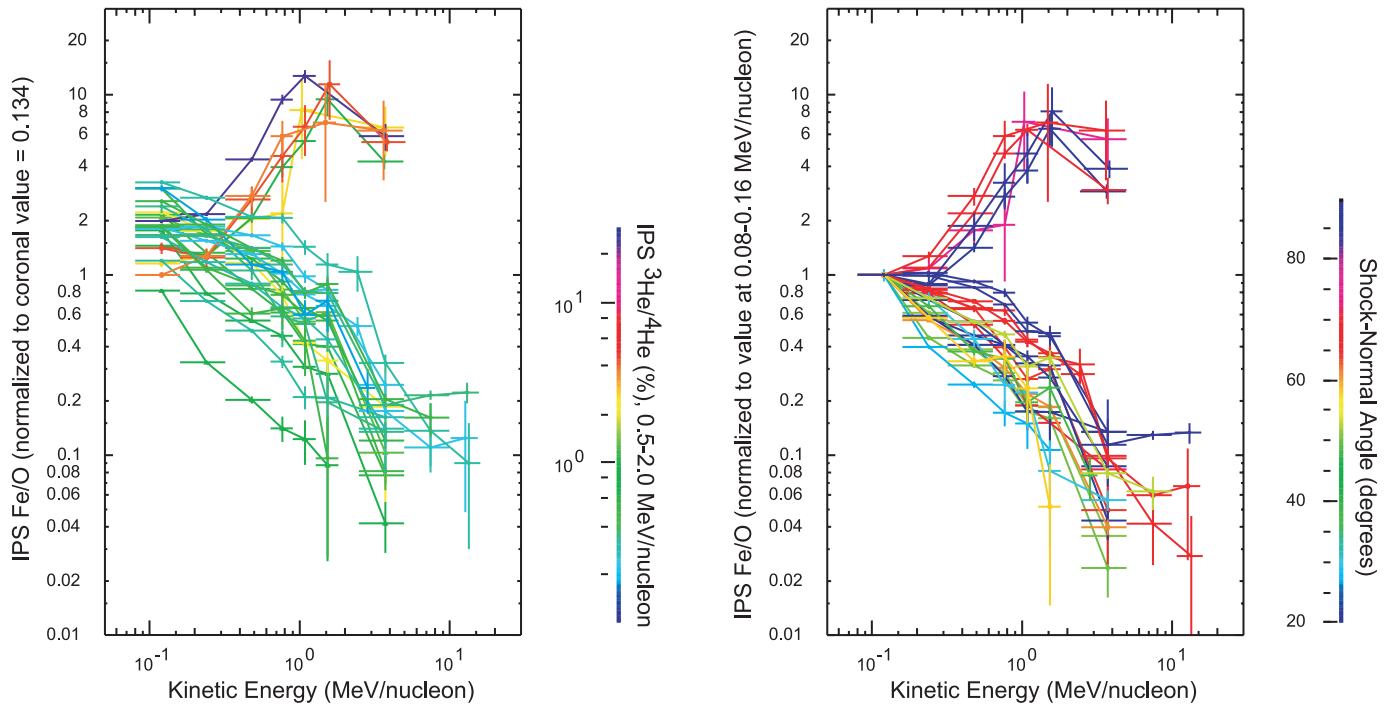

FIG. 3.—Fe/O vs. energy for 23 traveling IPS events (from Desai et al. 2003) in which the energy dependence is strong. Data points are from *ACE* ULEIS (~0.1–2.0 MeV nucleon^{-1}), *Wind* LEMT (~2.5–10 MeV nucleon^{-1}), and *ACE* SIS (10–15 MeV nucleon^{-1}). In the left panel, Fe/O is normalized to the nominal coronal value (0.134; Reames 1995), and the color indicates measured ^{3}He/^{4}He in the event at 0.5–2.0 MeV nucleon^{-1} from *ACE* ULEIS (Desai et al. 2003), as shown in the legend. (In eight of the events the result is actually an upper limit, as discussed in the text.) In the right panel, Fe/O is normalized to each event's observed value at 0.08–0.16 MeV nucleon^{-1}, and the color indicates the value of θ_{Bn} (or its supplement, if smaller) from *ACE*.

Figure 4, we therefore classify events with $\theta_{Bn} > 70^\circ$ as quasi-perpendicular and those with $\theta_{Bn} < 60^\circ$ as quasi-parallel. Similar demarcations were suggested by van Nes et al. (1984) and Tsurutani & Lin (1985) in their studies of electrons and protons locally accelerated by traveling interplanetary shocks.

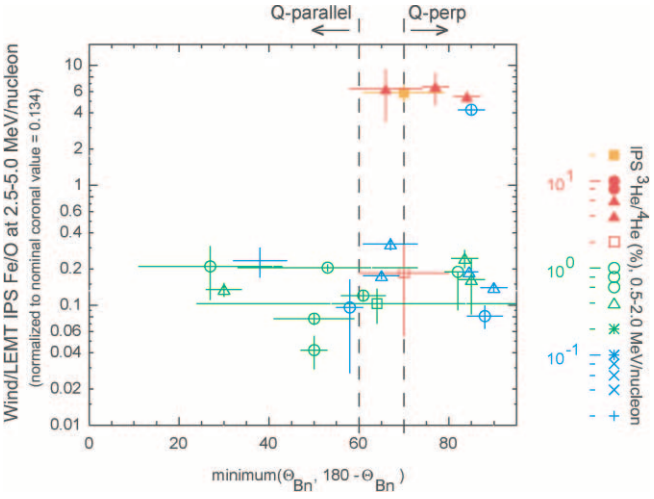

FIG. 4.—Correlation plot of each IPS event's Fe/O at 2.5–5.0 MeV nucleon^{-1} (from *Wind* LEMT) vs. the measured shock angle θ_{Bn} (from *ACE*). For the event at $\theta_{Bn} = 27^\circ \pm 16^\circ$, the plotted value is from highest energy at which Fe/O is available, at 1.3–1.8 MeV nucleon^{-1} (from *ACE* ULEIS). The Fe/O values are normalized to the reference value of 0.134 (Reames 1995). Since the polarity of the magnetic field vector is irrelevant here, the horizontal axis gives the minimum value of either θ_{Bn} or its supplement. Symbol shapes and color indicate ^{3}He/^{4}He from Desai et al. (2003), as given in the legend at the right, except for the eight symbols in blue, where the shape gives the 99% confidence-level upper limit, all of which are <0.65%. We classify shocks with $\theta_{Bn} < 60^\circ$ as quasi-parallel and shocks with $\theta_{Bn} > 70^\circ$ as quasi-perpendicular, as discussed in the text.

Among the noteworthy features of Figure 4 are the following:

1. There are six quasi-parallel IPS events with $\theta_{Bn} \lesssim 60^\circ$, plus one more in which the error bar on θ_{Bn} is large. All of these events have Fe/O that decreases with energy.
2. The five events with rising Fe/O may all be considered quasi-perpendicular, since four of them have $\theta_{Bn} \geq 70^\circ$ while the fifth has $\theta_{Bn} = 66^\circ \pm 8^\circ$.
3. Among the 18 events with falling-Fe/O, only one has ^{3}He/^{4}He exceeding 2%. For seven of these events, *ACE* ULEIS reported only a 3 σ upper limit for ^{3}He/^{4}He that was in all cases <0.52%. Among the other 11 events for which measurements are available, the weighted average is 0.54% ± 0.03%.
4. By contrast, four of the five events with rising Fe/O also have much larger ^{3}He/^{4}He, in the range ~3%–24%. In fact, these values are the largest in this event sample; they are ~70–600 times the solar-wind average, a clear indication that flare remnants are present in the seed population of these events. For the fifth event with rising Fe/O, *ACE* ULEIS reported an upper limit, ^{3}He/^{4}He < 0.65%. However, as already noted, Fe/O and ^{3}He/^{4}He enhancements in flares are not strictly correlated, so that this low ^{3}He/^{4}He does not rule out the possibility of enhanced Fe/O in the event's seed population.

Iron charge states are another indicator of seed population. The Solar Energetic Particle Charge Analyzer (SEPICA) on *ACE* has provided a list[15] of daily averaged values of $\langle Q_{Fe} \rangle$ at 0.23–0.30 MeV nucleon^{-1}. The list has results for 10 of the IPS events in this survey, including four events in which Fe/O increases with energy. Three of these four events have $\langle Q_{Fe} \rangle$ in the range 15.5 ± 3.6 to 17.7 ± 3.3, values generally associated with ions

[15] See http://www.srl.caltech.edu/ACE/ASC/DATA/level3/sepica/Fedaysteps_v11_level3.txt.

originating in flares. But the six events with decreasing Fe/O all have $\langle Q_{Fe} \rangle$ between 9.4 ± 0.4 and 11.8 ± 1.4.

Thus, although the correlations are not perfect, this event sample suggests a reasonably clear picture: Fe/O strongly increasing with energy preferentially corresponds to a quasi-perpendicular shock operating on a seed population with a significant component of flare suprathermals. However, these conditions may be necessary but not sufficient, and other factors, not revealed in this study, may also come into play. For example, Desai et al. (2004) have suggested that the detailed spectral characteristics of the seed population must also be taken into account.[16] (Mechanisms that may cause Fe/O to increase with energy will be discussed in § 5.) Moreover, one should recognize the statistical limitations of this analysis: the events with falling Fe/O are equally divided among those with $\theta_{Bn} \geq 65^\circ$ and those with $\theta_{Bn} < 65^\circ$. If the same distribution actually applied to the events with rising Fe/O, there is a ~3% chance that all five of them randomly appeared at $\theta_{Bn} > 65^\circ$.

Of course, it should also be emphasized that we are examining here only IPS events in which Fe/O has an extremely strong energy dependence. For most of the Desai et al. (2003) IPS events, the energy dependence is more gentle, but with Fe/O at various levels. (This is also true for most SEP events.) Among such events, different circumstances may have produced similar results. For example, Fe/O enhanced at all energies could occur if the injection threshold were sufficiently high that only flare-remnants could be accelerated by the shock *or* if the flare-remnants were simply so numerous that they dominated the seed population. Such events naturally make it difficult to identify potentially relevant factors; it is for this reason that we have focused on extreme events.

Finally, we examine more closely the events in which Fe/O decreases with energy. To do this, we took Fe/O versus energy at 0.08–1.3 MeV nucleon^{-1} and fitted it to an exponential of the form $\exp(\alpha E)$, where E is the energy and α is a fit parameter. In Figure 5 the fitted values of α are plotted versus θ_{Bn}. We have omitted events in which the uncertainty in θ_{Bn} is 10° or more. For the events at $\theta_{Bn} < 70^\circ$, there is a reasonably clear correlation, by which smaller θ_{Bn} corresponds to a steeper fall in Fe/O. Most of the events with $\theta_{Bn} > 80^\circ$ have a relatively slow falloff in Fe/O with energy. However, there are also two significant outliers above 80°, perhaps reflecting the case where the locally measured θ_{Bn} is not representative of the accelerator or other complexities among relevant factors at quasi-perpendicular shocks.

In summary, this sample of IPS events with strongly energy-dependent Fe/O is too small to provide definitive conclusions, especially when one considers the potential for obscuring complications. Nevertheless, these results suggest that both seed population and shock geometry play critical roles in this behavior.

3. SEP EVENTS AND SHOCK GEOMETRY

For SEP events we have no direct measure of θ_{Bn} when the CME-driven shock is still near the Sun. We must therefore rely on correlations among measurable quantities to test the plausibility of our hypothesis. Our notion is that flare ions in the seed population can effectively reveal the presence of a quasi-perpendicular shock. We therefore use Fe/O at 30–40 MeV nucleon^{-1} as a crude proxy for shock geometry, with enhanced Fe/O indicating a quasi-perpendicular shock. This particular energy bin is the highest at which we have measurable Fe/O in a large number of events.

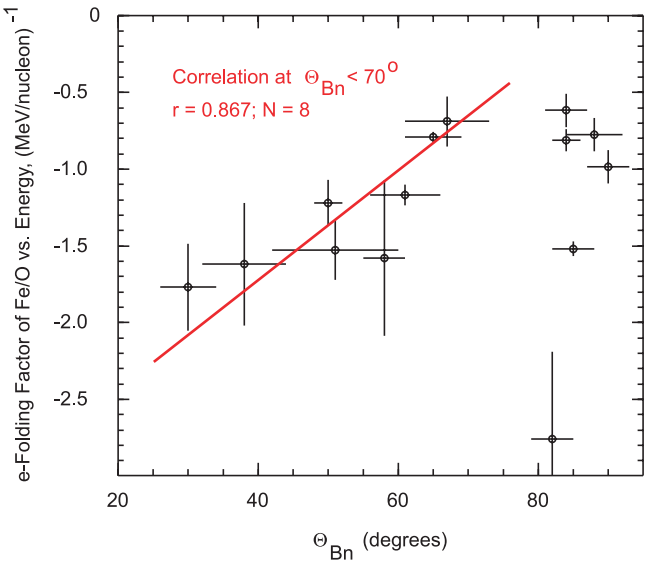

FIG. 5.—Correlation plot of α vs. θ_{Bn}, where α is determined from a fit of Fe/O vs. energy at 0.08–1.3 MeV nucleon^{-1} to the form $\exp(\alpha E)$ for IPS events in which Fe/O decreases with energy E. Events in which the uncertainty in θ_{Bn} is 10° or more have been omitted. The correlation fit is only to events with $\theta_{Bn} < 70^\circ$. The correlation coefficient $r = 0.867$ for $N = 8$ data points corresponds to a random probability of <0.5%.

To identify SEP events for this study, we examined protons above 30 MeV, as reported by *GOES-8* or (after 2003 April 12) *GOES-11*. Our sole selection criterion was that the event-integrated fluence of >30 MeV protons exceed 2×10^5 cm^{-2} sr^{-1}. This energy biases our measure of size toward particles accelerated near the Sun (Cane et al. 2003). This fluence threshold selects events for which the >30 MeV proton fluence was ~20 times larger than that of the biggest impulsive event of cycle 23 (2002 August 20: Leske et al. 2003; Reames & Ng 2004).

Between 1997 November 1 and 2004 April 30, we found 44 events that met this criterion. *ACE* SIS is sufficiently large that it measured Fe and O above 30 MeV nucleon^{-1} in all but one of these events. (That one event had its associated flare at heliolongitude E79°.) Since the selection was made on the basis of protons alone, this event sample provides an essentially unbiased survey of high-energy heavy-ion characteristics in the large solar proton events of solar cycle 23. Table 1 lists the events, including the associated CME speed, source longitude, >30 MeV proton fluence, and whether or not the event was a GLE. The table also gives the value of Fe/O at 30–40 MeV nucleon^{-1} from *ACE* SIS and, for comparison, at 3.2–5.0 MeV nucleon^{-1} from *Wind* LEMT. The table also contains spectral information for oxygen and iron, as will be discussed below. Throughout this analysis, estimates of contemporaneous Galactic cosmic rays (as modeled from 27 day averages from the Cosmic Ray Isotope Spectrometer on *ACE* [Stone et al. 1998b]) and anomalous cosmic rays (from solar-quiet observations from *ACE* SIS [Leske et al. 2000] and *Wind* LEMT [Reames & MacDonald 2003]) have been subtracted from the measured intensities.

3.1. *Event Size*

Event size can be influenced by a number of factors, including shock geometry. Because quasi-perpendicular shocks tend to

[16] For each of the IPS events, Desai et al. (2003) identified a preceding "upstream" time interval whose characteristics they believe to be representative of the shock's seed population. In one of the events in which Fe/O increases with energy (number 37 from their list), they found the same energy dependence in Fe/O at the shock and in the upstream interval, so that the ratio of Fe/O at the shock to Fe/O in the upstream interval was independent of energy, at least at ~0.1–1.0 MeV nucleon^{-1}. However, this behavior was not observed in the other events in which Fe/O increases with energy.

TABLE 1

LARGE GRADUAL SOLAR ENERGETIC PARTICLE EVENTS OF SOLAR CYCLE 23

						Fe/O/0.134[a]		OXYGEN POWER-LAW INDEX		IRON POWER-LAW INDEX	
EVENT NO. (1)	EVENT INTERVAL[b] (2)	CME SPEED[c] (km s^{-1}) (3)	SOURCE LOCATION[d] (deg) (4)	>30 MeV PROTON FLUENCE[e] (cm^{-2} sr^{-1}) (5)	GLE[f] (6)	*Wind* LEMT (3.2–5.0 MeV nucleon^{-1}) (7)	*ACE* SIS (30–40 MeV nucleon^{-1}) (8)	*Wind* LEMT (3–10 MeV nucleon^{-1}) (9)	*ACE* SIS (30–100 MeV nucleon^{-1}) (10)	*Wind* LEMT (3–10 MeV nucleon^{-1}) (11)	*ACE* SIS (21–100 MeV nucleon^{-1}) (12)
1.....	1997 Nov 4 07:00–1997 Nov 6 11:00	785	S14, W33	6.71e+05	N	4.23 ± 0.05	3.03 ± 0.23	2.75 ± 0.08	3.16 ± 0.39	2.37 ± 0.08	3.36 ± 0.20
2.....	1997 Nov 6 14:00–1997 Nov 10 00:00	1556	S18, W63	1.22e+07	Y	3.15 ± 0.02	5.78 ± 0.10	2.53 ± 0.08	2.48 ± 0.12	1.78 ± 0.08	2.43 ± 0.07
3.....	1998 Apr 20 12:00–1998 Apr 26 00:00	1863	S, W90	2.77e+07	N	2.13 ± 0.01	0.019 ± 0.003	1.16 ± 0.08	6.43 ± 0.33	2.64 ± 0.08	8.04 ± 0.60
4.....	1998 May 2 14:00–1998 May 4 00:00	938	S15, W15	1.50e+06	Y	5.03 ± 0.11	4.93 ± 0.32	2.36 ± 0.07	2.39 ± 0.19	1.78 ± 0.09	2.45 ± 0.15
5.....	1998 May 6 08:00–1998 May 8 12:00	1099	S11, W65	6.55e+05	Y	4.53 ± 0.06	3.99 ± 0.44	2.99 ± 0.08	3.16 ± 0.18	2.44 ± 0.09	4.24 ± 0.33
6.....	1998 Aug 24 23:00–1998 Aug 27 18:00	...	N35, E09	3.65e+06	Y	0.406 ± 0.006	0.84 ± 0.09	3.28 ± 0.08	6.27 ± 0.45	3.27 ± 0.11	2.04 ± 0.20
7.....	1998 Sep 30 14:00–1998 Oct 3 00:00	...	N19, W85	3.50e+06	N	1.62 ± 0.01	1.68 ± 0.07	2.55 ± 0.08	4.05 ± 0.19	2.02 ± 0.09	3.77 ± 0.12
8.....	1998 Nov 14 07:00–1998 Nov 17 00:00	...	N, W120	2.51e+06	N	3.70 ± 0.03	4.46 ± 0.13	2.00 ± 0.08	3.85 ± 0.19	1.50 ± 0.09	3.34 ± 0.09
9.....	1999 Jun 1 20:00–1999 Jun 4 06:00	1772	N, W120	4.20e+05	N	0.83 ± 0.02	4.73 ± 0.30	2.37 ± 0.08	2.69 ± 0.24	1.46 ± 0.09	2.73 ± 0.13
10.....	1999 Jun 4 0800–1999 Jun 8 00:00	2230	N17, W69	2.45e+05	N	0.80 ± 0.01	2.50 ± 0.35	3.81 ± 0.08	4.91 ± 0.73	3.21 ± 0.09	3.45 ± 0.30
11.....	2000 Jun 10 18:00–2000 Jun 13 12:00	1108	N22, W40	2.95e+05	N	5.03 ± 0.15	4.56 ± 0.68	2.94 ± 0.09	4.39 ± 0.69	2.31 ± 0.10	3.45 ± 0.26
12.....	2000 Jul 14 11:00–2000 Jul 17 00:00	1674	N22, W07	3.42e+08	Y	3.97 ± 0.01	0.57 ± 0.02	1.08 ± 0.08	4.83 ± 0.19	1.72 ± 0.08	3.73 ± 0.12
13.....	2000 Sep 12 13:00–2000 Sep 16 12:00	1550	S17, W09	9.42e+05	N	0.242 ± 0.003	3.10 ± 0.53	3.99 ± 0.08	4.25 ± 0.64	3.39 ± 0.10	4.07 ± 0.40
14.....	2000 Oct 16 08:00–2000 Oct 20 12:00	1336	N, W95	2.02e+05	N	3.36 ± 0.06	5.02 ± 1.81	2.56 ± 0.08	3.36 ± 0.47	2.02 ± 0.09	3.65 ± 0.23
15.....	2000 Nov 8 23:00–2000 Nov 11 12:00	1345	N10, W75	2.53e+08	N	3.22 ± 0.01	0.041 ± 0.006	1.63 ± 0.08	4.67 ± 0.17	1.92 ± 0.08	7.16 ± 1.04
16[g].....	2000 Nov 24 0600–2000 Nov 28 12:00	994	N22, W07	3.62e+06	N	1.10 ± 0.01	0.69 ± 0.04	2.72 ± 0.08	4.95 ± 0.24	2.41 ± 0.09	4.19 ± 0.21
17.....	2001 Jan 28 1800–2001 Feb 1 00:00	916	S04, W59	2.86e+05	N	1.83 ± 0.04	4.36 ± 0.60	3.70 ± 0.08	3.92 ± 0.58	2.64 ± 0.10	3.54 ± 0.26
18.....	2001 Mar 29 12:00–2001 Apr 1 06:00	942	N16, W12	2.83e+05	N	3.35 ± 0.04	2.63 ± 0.25	2.78 ± 0.08	4.13 ± 0.42	2.48 ± 0.09	4.06 ± 0.25
19.....	2001 Apr 2 23:00–2001 Apr 6 00:00	2505	N17, W78	7.62e+06	N	2.42 ± 0.01	1.90 ± 0.05	2.12 ± 0.08	3.90 ± 0.15	2.06 ± 0.08	3.64 ± 0.09
20.....	2001 Apr 10 08:00 –2001 Apr 12 12:00	2411	S23, W09	1.52e+06	N	0.88 ± 0.01	0.76 ± 0.04	3.24 ± 0.08	4.78 ± 0.20	2.68 ± 0.09	5.13 ± 0.23
21.....	2001 Apr 12 12:00–2001 Apr 14 16:00	1184	S20, W42	5.14e+05	N	0.90 ± 0.02	1.58 ± 0.55	3.59 ± 0.08	4.40 ± 0.92	3.24 ± 0.11	4.02 ± 0.58
22.....	2001 Apr 15 14:00–2001 Apr 18 04:00	1199	S20, W84	1.16e+07	Y	2.55 ± 0.02	4.78 ± 0.19	2.61 ± 0.08	2.51 ± 0.15	2.31 ± 0.09	2.20 ± 0.08
23.....	2001 Apr 18 04:00–2001 Apr 22 00:00	2465	S W120	3.56e+06	Y	1.55 ± 0.02	2.95 ± 0.19	2.50 ± 0.08	3.14 ± 0.22	2.46 ± 0.09	2.40 ± 0.11
24.....	2001 Aug 16 01:00–2001 Aug 19 00:00	1575	W140, ?	7.37e+06	N	1.33 ± 0.02	0.80 ± 0.03	1.48 ± 0.08	3.63 ± 0.16	1.45 ± 0.09	3.51 ± 0.11
25.....	2001 Sep 24 11:00–2001 Sep 30 00:00	2402	S16, E23	9.74e+07	N	0.96 ± 0.01	0.091 ± 0.006	2.06 ± 0.08	5.08 ± 0.16	2.17 ± 0.09	5.69 ± 0.30

TABLE 1—*Continued*

Event No. (1)	Event Interval[b] (2)	CME Speed[c] (km s^{-1}) (3)	Source Location[d] (deg) (4)	>30 MeV Proton Fluence[e] (cm^{-2} sr^{-1}) (5)	GLE[f] (6)	Fe/O/0.134[a]		Oxygen Power-Law Index		Iron Power-Law Index	
						Wind LEMT (3.2–5.0 MeV nucleon^{-1}) (7)	*ACE* SIS (30–40 MeV nucleon^{-1}) (8)	*Wind* LEMT (3–10 MeV nucleon^{-1}) (9)	*ACE* SIS (30–100 MeV nucleon^{-1}) (10)	*Wind* LEMT (3–10 MeV nucleon^{-1}) (11)	*ACE* SIS (21–100 MeV nucleon^{-1}) (12)
26.....	2001 Oct 1 13:00–2001 Oct 5 00:00	1405	S20, W88	6.73e+06	N	0.55 ± 0.04	0.50 ± 0.12	1.99 ± 0.08	6.91 ± 0.49	3.02 ± 0.10	3.86 ± 0.55
27.....	2001 Oct 22 16:00–2001 Oct 26 12:00	1336	S21, E18	3.64e+05	N	1.06 ± 0.05	5.69 ± 1.06	3.57 ± 0.09	3.08 ± 0.67	2.09 ± 0.12	2.43 ± 0.26
28.....	2001 Nov 4 17:00–2001 Nov 9 00:00	1810	N06, W18	2.71e+08	Y	1.80 ± 0.01	0.31 ± 0.03	1.16 ± 0.08	4.16 ± 0.20	2.02 ± 0.09	3.52 ± 0.24
29.....	2001 Nov 22 21:00–2001 Nov 26 00:00	1443	S15, W34	6.74e+07	N	1.10 ± 0.003	0.45 ± 0.03	2.16 ± 0.08	5.08 ± 0.22	2.76 ± 0.09	4.13 ± 0.22
30.....	2001 Dec 26 06:00–2001 Dec 29 09:00	1406	N08, W54	6.67e+06	Y	1.49 ± 0.01	4.18 ± 0.12	2.52 ± 0.08	3.01 ± 0.16	1.81 ± 0.09	2.70 ± 0.09
31[h].....	2001 Dec 30 12:00–2002 Jan 4 00:00	?	?	7.62e+05	N	0.68 ± 0.01	0.19 ± 0.05	2.83 ± 0.08	7.61 ± 0.70	3.11 ± 0.09	6.20 ± 1.26
32[i].....	2002 Jan 10 00:00–2002 Jan 14 00:00	1794	S18, E79	2.69e+05	N	0.115 ± 0.004	...	3.72 ± 0.08	...	4.54 ± 0.20	...
33.....	2002 Apr 21 00:00–2002 Apr 24 00:00	2409	S14, W84	5.28e+07	N	1.31 ± 0.004	0.14 ± 0.01	1.83 ± 0.08	5.95 ± 0.19	2.15 ± 0.08	5.40 ± 0.25
34.....	2002 May 22 06:00–2002 May 25 00:00	1494	S22, W53	3.52e+05	N	0.281 ± 0.005	0.43 ± 0.07	3.59 ± 0.08	4.85 ± 0.39	2.40 ± 0.09	5.53 ± 0.50
35[i].....	2002 Jul 16 12:00–2002 Jul 19 00:00	1132	N19, W01	2.53e+05	N	0.47 ± 0.01	0.88 ± 0.22	3.44 ± 0.08	5.44 ± 0.65	2.58 ± 0.10	3.52 ± 0.95
36.....	2002 Jul 21 00:00–2002 Jul 26 00:00	1941	S E90	5.13e+05	N	0.62 ± 0.01	0.56 ± 0.10	2.41 ± 0.08	5.69 ± 0.43	2.35 ± 0.09	3.70 ± 0.45
37.....	2002 Aug 22 00:00–2002 Aug 24 00:00	1005	S07, W62	4.08e+05	N	...	4.64 ± 0.75	...	3.98 ± 0.68	...	3.55 ± 0.29
38.....	2002 Aug 24 00:00–2002 Aug 27 00:00	1878	S02, W81	3.86e+06	Y	1.17 ± 0.01	4.61 ± 0.26	2.96 ± 0.07	3.33 ± 0.23	2.55 ± 0.09	2.79 ± 0.11
39.....	2002 Nov 9 14:00–2002 Nov 12 00:00	1838	S12, W29	4.28e+05	N	0.93 ± 0.01	0.25 ± 0.12	3.00 ± 0.08	6.01 ± 0.54	3.44 ± 0.09	6.01 ± 0.30
40.....	2003 Oct 26 18:00–2003 Oct 28 00:00	1537	N02, W38	1.46e+06	N	1.58 ± 0.01	1.21 ± 0.08	2.43 ± 0.08	3.59 ± 0.17	2.51 ± 0.09	3.55 ± 0.13
41.....	2003 Oct 28 11:00–2003 Oct 29 16:00	2459	S16, E08	2.43e+08	Y	4.36 ± 0.01	0.068 ± 0.012	0.80 ± 0.08	4.82 ± 0.18	1.88 ± 0.08	3.31 ± 0.26
42.....	2003 Oct 29 21:00–2003 Nov 2 00:00	2029	S15, W02	4.16e+07	Y	2.50 ± 0.01	0.83 ± 0.04	1.78 ± 0.08	4.05 ± 0.16	2.05 ± 0.08	3.40 ± 0.10
43.....	2003 Nov 2 17:00–2003 Nov 4 20:00	2598	S14, W56	1.56e+07	Y	1.10 ± 0.003	0.57 ± 0.04	1.93 ± 0.08	4.87 ± 0.18	2.58 ± 0.08	3.84 ± 0.14
44.....	2003 Nov 4 21:00–2003 Nov 8 00:00	2657	S19, W83	2.58e+06	N	0.598 ± 0.004	0.44 ± 0.05	3.18 ± 0.08	5.42 ± 0.26	3.40 ± 0.09	3.97 ± 0.26

[a] Normalized to the nominal coronal value, 0.134 (Reames 1995).
[b] Date and UT of start and stop of the integration interval.
[c] From one-parameter fits to the LASCO time-height profiles, as given by http://cdaw.gsfc.nasa.gov/CME_list. The measured speeds do not take into account potential projection effects. The Web site does not report error bars on the fitted speeds, but comparisons of results from independent analyses of the LASCO images suggest that the uncertainties are likely to be on the order of 10%–20% (M. Andrews, A. Reinard, S. Kahler, & S. Yashiro 2004, private communications).
[d] From Cane et al. (2002, 2003) whenever possible; later events from *Solar Geophysical Data* or other sources, as detailed in the text.
[e] From *GOES-8* or (in 2003) *GOES-11*. Read "2.00e+07" as 2.00×10^7. The event selection required this fluence to be greater than 2.0×10^5 protons cm^{-2} sr^{-1}.
[f] N = no; Y = reported by least one neutron monitor station.
[g] Multiple events.
[h] Solar source not identified (Gopalswamy 2003).
[i] Delayed onset at 1 AU. Flare and CME associations provided by http://umbra.nascom.nasa.gov/SEP/seps.html.

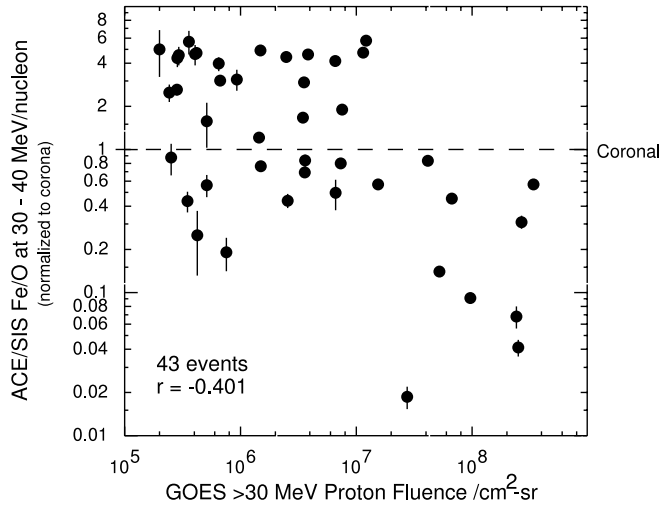

FIG. 6.—Correlation of event-integrated Fe/O at 30–40 MeV nucleon^{-1} from *ACE* SIS vs. the event-integrated proton fluence above 30 MeV from *GOES*. The correlation coefficient between these variables is −0.401.

require a higher injection energy, they generally draw from a smaller seed population than quasi-parallel shocks. Therefore, unless the overall injection efficiency is significantly higher for quasi-perpendicular shocks (which is unlikely), we would generally expect quasi-perpendicular events to have smaller fluences than quasi-parallel events. Van Nes et al. (1984) noted that the largest traveling IPS events had $30^\circ < \theta_{Bn} < 60^\circ$. Desai et al. (2004) found that the IPS events with Fe/O increasing with energy were among the smallest events in their sample.

Figure 6 shows the correlation of high-energy Fe/O versus event size, as measured by the event-integrated proton fluence above 30 MeV. The events with enhanced Fe/O tend to have smaller fluences. High-energy Fe/O is not enhanced in any of the largest events, in which the fluence exceeds $\sim 2 \times 10^7$ protons cm^{-1} sr^{-1}. Given the many factors that can affect event size, one should not conclude that Fe-rich events *cannot* have large fluences. (The extraordinary SEP events of 1989 September and October [Tylka & Dietrich 1999] come to mind.) Rather, Figure 6 suggests that enhanced high-energy Fe/O is rare among the largest events.

(Among these very large fluence events are three far-western events, 1998 April 20 [W90° with 2.8×10^7 protons cm^{-2} sr^{-1} above 30 MeV], 2000 November 8 [W75°, 2.5×10^8 protons cm^{-1} sr^{-1}], and 2002 April 21 [W84°, 5.3×10^7 protons cm^{-2} sr^{-1}]. In these events, the >30 MeV fluence was not significantly increased when the flank of the shock arrived at Earth. These events contradict the often-heard assertion that very large fluences are found *only* in events from near central meridian, with a large shock-related increase at 1 AU.)

It should be noted that if enhanced high-energy Fe/O were *solely* due to a seed population augmented by flare particles, with no other factors coming into play, we should expect the Fe-rich events to be larger, at least on average. This is not what we see in Figure 6.

3.2. *Spectral Characteristics*

Shock geometry has important consequences for spectral shape. In particular, the upstream magnetic field is one of the factors controlling escape from the shock region, with the quasi-perpendicular geometry tending to retain particles in the shock region and thereby producing harder spectra at high energies. One therefore expects the *e*-folding energy E_0 in $F(E) \sim E^{-\gamma} \exp(-E/E_0)$ to scale as something like $(\sec \theta_{Bn})^{2/(2\gamma-1)}$ (Lee 2005), where γ is the power-law index at the shock. Thus, in general, one would expect quasi-perpendicular shocks to show less pronounced spectral rollovers at high energies and to be more like power laws.

The top half of Figure 7 shows time-dependent oxygen spectra from *ACE* SIS at 10–90 MeV nucleon^{-1} covering the first 7 hr of the 2002 April 21 and 2002 August 24 events. During the first hour of the events, there is no discernible difference between the spectra within this limited energy range, except for size. After that, the spectral differences are clear: the candidate quasi-parallel event (April) is larger and has a relatively soft spectrum at the highest energies, while the candidate quasi-perpendicular event (August) is smaller but with a relatively hard spectrum. These differences are evident from almost the very beginning, suggesting that they do indeed reflect inherent characteristics of the accelerator while near the Sun.

The bottom half of Figure 7 shows iron spectra for these same time periods. The qualitative difference in the spectral character of the two events is again evident. One also sees that in the April event, iron above ~20 MeV nucleon^{-1} has a softer spectrum than oxygen from the very beginning. By contrast, in the August event, oxygen and iron have nearly identical spectral shapes in the first 3 hr. After that, iron is clearly harder than oxygen.

Figure 8 shows event-averaged oxygen and iron spectra for these two events. Of course, event-averaged spectra integrate over evolution in the shock geometry as the shock moves outward. Nevertheless, for both species, the departure from a power law is clearly more severe at the highest energies in the April event than in the August event. Figure 8 also reveals the spectral origin of the compositional differences in Figure 1: in the April event, Fe at high-energies rolls over more steeply than oxygen. But in the August event, at high energies Fe has a harder power law than oxygen (Tylka et al. 2002).

We now focus on the oxygen spectrum since, unlike Fe, its interpretation is not potentially complicated by a wide range of Q/A values. (We discuss Fe spectra further in § 4.2.) To characterize spectral steepening in other events, we fit portions of the event-averaged oxygen spectra to two independent power laws, one ($E^{-\gamma_1}$) at 3–10 MeV nucleon^{-1} and the other ($E^{-\gamma_2}$) at 30–100 MeV nucleon^{-1}. Data for the former come from *Wind* LEMT; for the latter, primarily from *ACE* SIS but with a few additional measurements from the University of Chicago's Cosmic Ray Nuclei Experiment (CRNE; Garcia-Munoz et al. 1975) on *IMP8* in the larger events (Tylka & Dietrich 1999; Tylka et al. 2002). The values of γ_1 and γ_2 are listed in columns (9) and (10) of Table 1. The spectra are not necessarily broken power laws. Nevertheless, as illustrated schematically in the left panel of Figure 8, we can use the difference between these indices, $\gamma_2 - \gamma_1$, to provide a measure of spectral steepening. For a weak spectral rollover (the quasi-perpendicular case), we would expect $\gamma_2 - \gamma_1 \sim 0$. However, for a strong rollover (the quasi-parallel case), $\gamma_2 - \gamma_1 > 0$.

We would therefore expect an anticorrelation between $\gamma_2 - \gamma_1$ and the high-energy Fe/O. This anticorrelation is indeed what we see in Figure 9.

It is important to remember that there are no selection biases in Figure 9: the events were chosen on the basis of proton fluence and without reference to their heavy-ion characteristics. One might also worry about "innate" biases, arising from the role of oxygen in the quantities on both axes. But a moment's thought shows that the trends in Figure 9 are the opposite from what one might expect on that basis: the *softest* high-energy oxygen

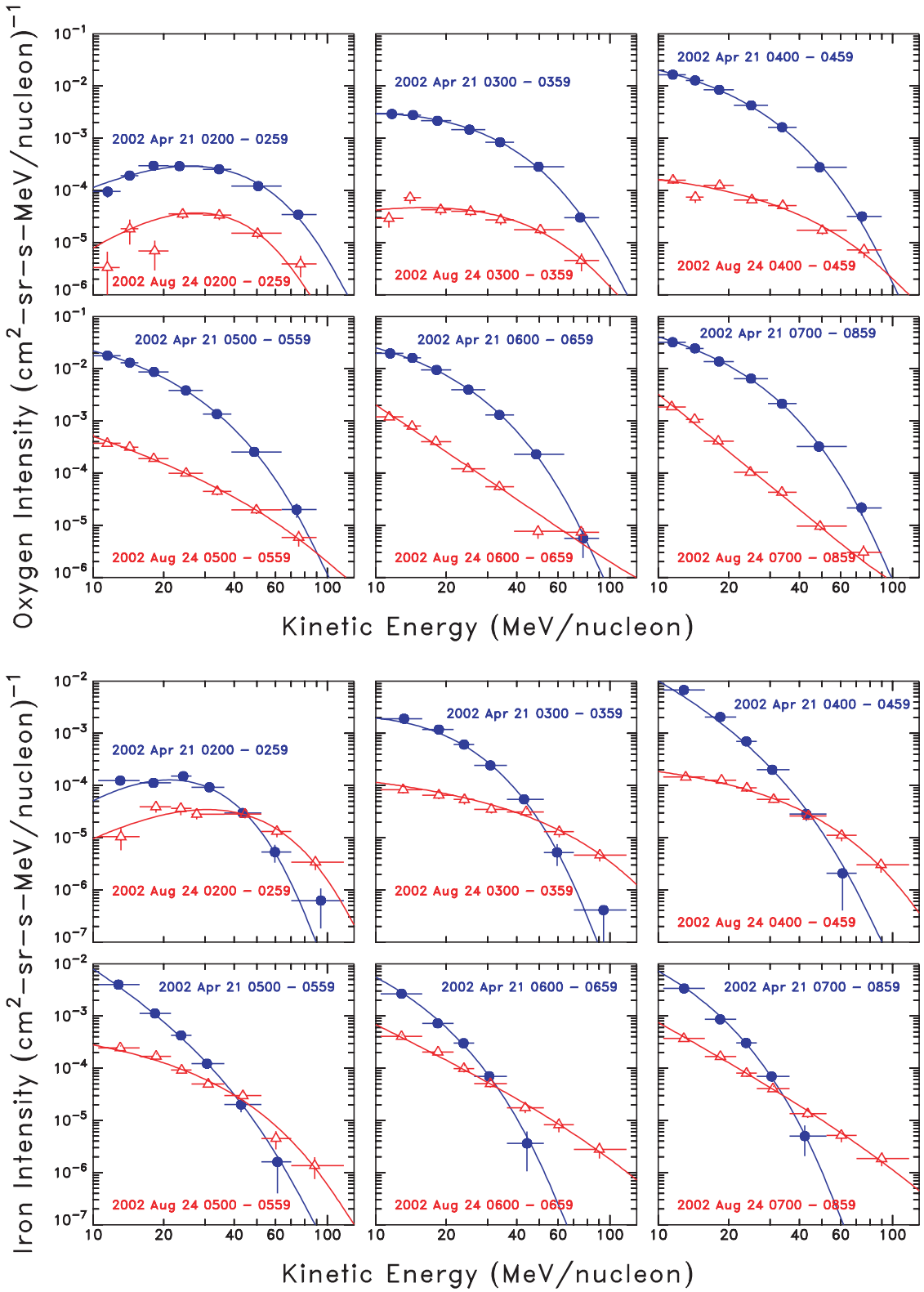

FIG. 7.—Temporal evolution in oxygen (*top*) and iron (*bottom*) spectra at >10 MeV nucleon^{-1} from *ACE* SIS in the 2002 April 21 (*blue*, *filled circles*) and 2002 August 24 (*red*, *open triangles*) events. The panels cover the first 7 hr of the events. (Coincidentally, the two events began at nearly the same UT: the starts of the *GOES* soft X-rays were at 0043 and 0049 UT, respectively; the estimated launch times of the CMEs were 0117 and 0057 UT, respectively; reported onsets of the metric type II bursts were 0118 and 0101 UT, respectively; and >100 MeV protons were first detected above 0.1 p cm^{-2} sr^{-1} s^{-1} on *GOES* at 0145 and 0125 UT, respectively. Thus, spectra at the same UT are at comparable points in the events' evolution.) The curves are fits to the functional form $F(E) \sim E^{-\gamma} \exp(-E/E_0)$, which roughly describes the data.

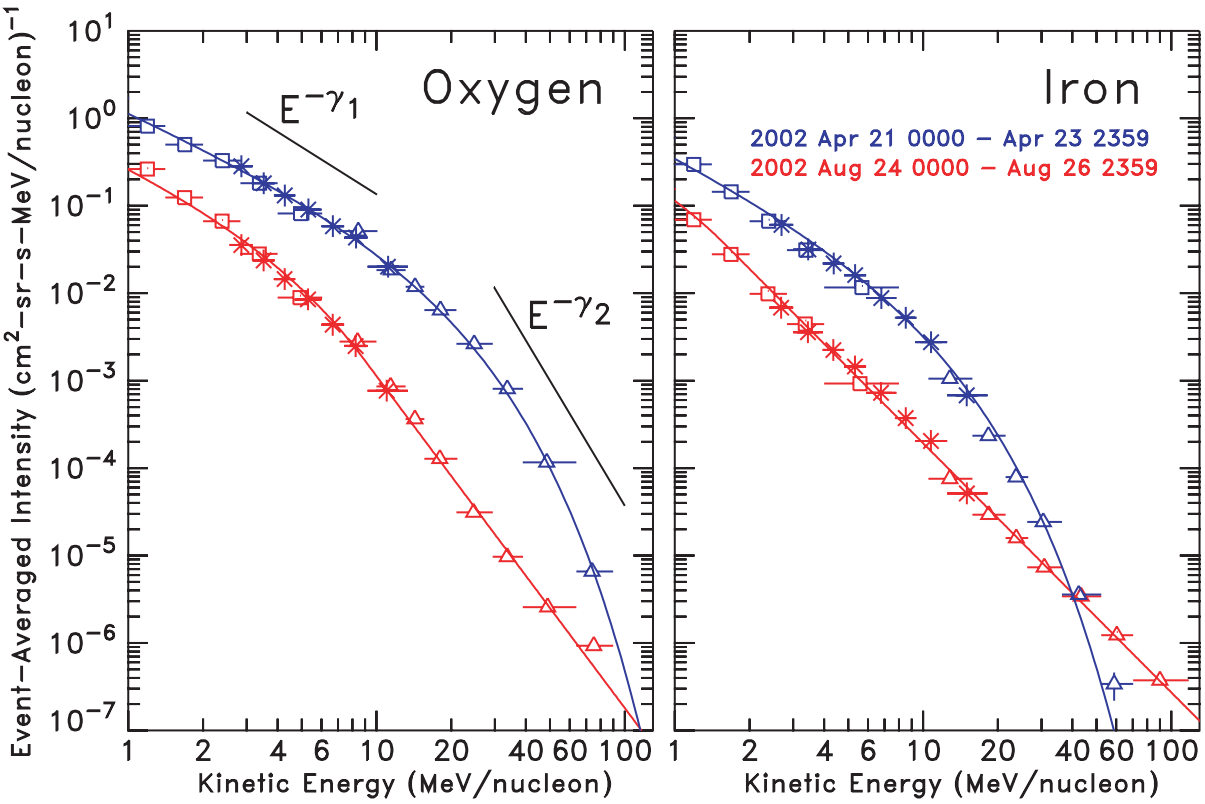

FIG. 8.—Event-averaged oxygen (*left panel*) and iron (*right panel*) spectra in the 2002 April 21 (*blue*) and 2002 August 24 (*red*) events. Symbols are as in Fig. 1. The curves through the data points are fits to the Ellison & Ramaty functional form (for the April event) and the double power law Band et al. (1993) functional form (for the August event). Power-law fits at 3–10 MeV nucleon^{-1} ($E^{-\gamma_1}$) and 30–100 MeV nucleon^{-1} ($E^{-\gamma_2}$) are used to quantify the spectral steepening, as described in the text.

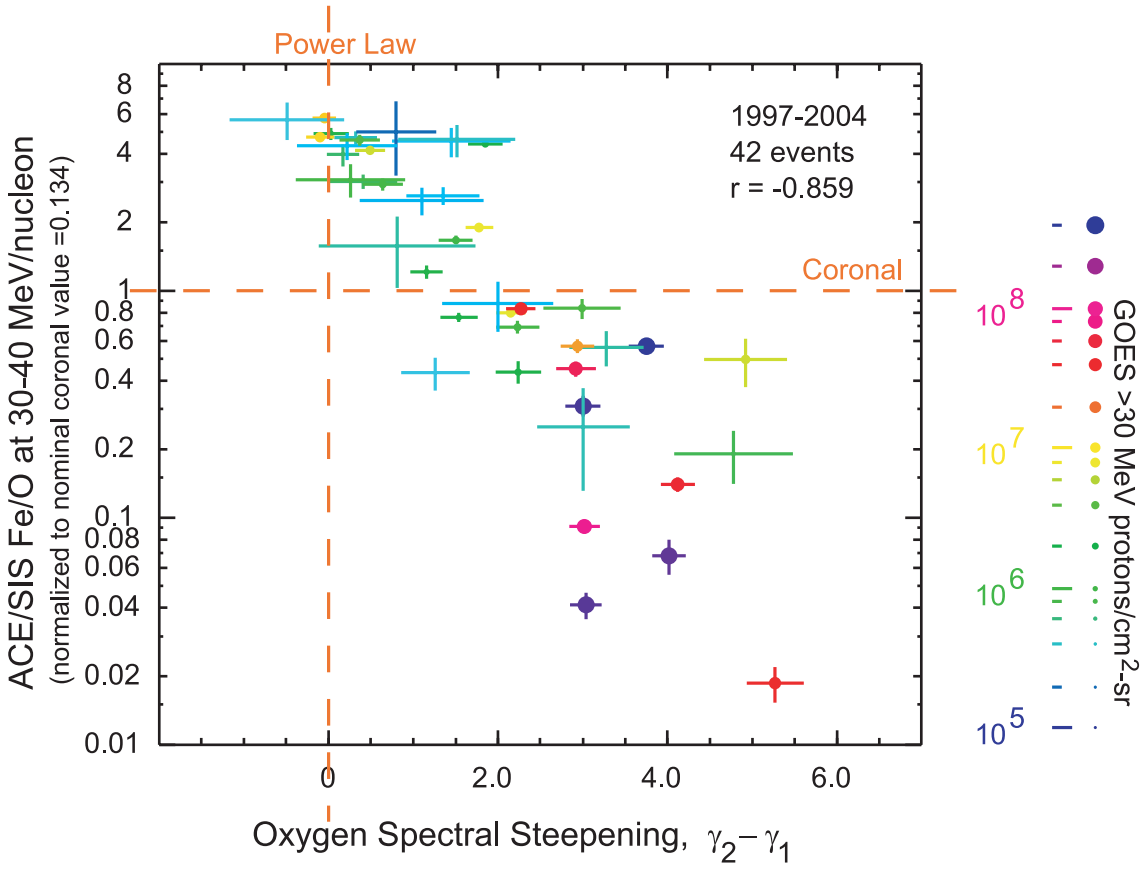

FIG. 9.—Correlation of event-integrated Fe/O at 30–40 MeV nucleon^{-1} vs. spectral steepening of the oxygen spectrum, as described in the text. The weighted correlation coefficient for these data points is −0.859. The Fe-rich events tend to be more like power laws. One of the events from Table 1 (2002 August 22) is missing because of a partial *Wind* data gap. The symbol size and color indicate the event-integrated fluence of >30 MeV protons from *GOES*, as given in the legend at the right.

spectra (on the right side of the plot) correspond to *suppressed* Fe/O.

The weighted correlation coefficient for the data points in Figure 9 is −0.859; for uncorrelated variables, this value corresponds to random probability of $<10^{-5}$. Accordingly, the correlation is highly significant. There are no events in the upper right, corresponding to strong Fe enhancements while the oxygen spectrum steeply rolls over; and there are no events in the lower left, where Fe would be suppressed while oxygen was nearly a power-law spectrum. As we have already noted, these correlations fall out naturally from our hypothesized connection between shock geometry and accessible seed populations. The behavior in Figure 9 is also a powerful constraint for alternative hypotheses and future SEP modeling efforts.

It is interesting to note that Figure 9 shows no events with a statistically significant level of spectral hardening, that is, $\gamma_2 - \gamma_1 < 0$. In general one would expect to see spectral hardening if two distinct acceleration mechanisms, with one mechanism substantially more prolific at accelerating to high energies, were operating. (This point is discussed further in § 4.2.)

3.3. *Presence of* GeV *Particles*

As already noted, quasi-perpendicular shocks are particularly effective at producing GeV particles. According to our hypothesis, we would therefore generally expect GLEs to be Fe-rich at high energies. This expectation need not always be true, in that flare Fe might not be available in the seed population of some events. Using data from the *IMP8* CRNE, Dietrich & Lopate (1999) first reported a tendency for GLEs to have enhanced Fe/O above ∼50 MeV nucleon^{-1}.

Table 2 summarizes *IMP8* CRNE observations of high-energy Fe/O for 25 GLEs of solar cycles 21 and 22. The table includes the numbers of Fe and O ions from roughly commensurate energy bins, as well as the Fe/O ratio. Most of the Fe/O measurements are at 47–80 MeV nucleon^{-1}. The numbers of Fe ions at this energy have been corrected for a priority scheme that telemeters only two-thirds of them compared to the oxygen ions, which come to rest at a deeper level in the detector stack. As noted in the table, a few of the Fe/O results are at 97–175 MeV nucleon^{-1}, where no priority corrections are required. In all of these events, instrumental backgrounds and the expected numbers of Galactic Fe ions are negligible, generally <0.01, and in no case more than 0.15 ion. By examining particle time-intensity profiles prior to each event, we found one GLE (1979 August 21) in which the high-energy Fe ions were dominated by the decay phase of an earlier SEP event. That GLE was dropped from the analysis and is not listed in Table 2. Otherwise, none of the GLEs in Table 2 had a significant contamination of high-energy Fe ions from preceding SEP events.

There are five GLEs in Table 2 (numbers 34, 35, 37, 40, and 50) in which *IMP8* CRNE collected fewer than 10 oxygen ions. In these five events, the Fe/O ratio is enhanced compared to the nominal coronal value of 0.134 (Reames 1995), at least on average: adding up the numbers of ions in those events in Table 2, one finds ∼22 iron ions and 21 oxygen ions. Setting aside these low-statistics GLEs, 18 of the remaining 20 GLEs (that is, 90%) have Fe/O that is enhanced relative to the nominal coronal value by a factor of 2 or more. In two of these events (numbers 36 and 42), Fe/O rises with energy so that the enhancement does not become evident until the higher energy bin at ≳100 MeV nucleon^{-1}.

Figure 10 shows event-integrated Fe/O measurements from *Wind* LEMT, *ACE* SIS, and *IMP8* CRNE at 3–197 MeV nucleon^{-1} in the 13 GLEs of 1997–2003. These events exhibit a wide range of behaviors when viewed over this energy range. The most complicated energy dependence, in which Fe/O drops and then rises at the highest energies, is most often observed in events with source regions near the center of the solar disk. The events with western source longitudes tend to have simpler energy dependence.

For the purposes of this discussion, we focus on high energies, above ∼40 MeV nucleon^{-1}. Prior to 2003 October, solar cycle 23 GLEs were consistent with the event statistics of cycles 21 and 22: eight of the 10 events showed enhanced Fe/O at ∼40 MeV nucleon^{-1}, and in another one (2000 July 14), the enhancement became apparent at higher energies. Only one of these 10 events (2001 November 4) failed to exhibit enhanced Fe/O at high-energy.[17] However, the three exceptionally powerful events that arose from the same active region on 2003 October 28–November 2 did not attain strong high-energy Fe/O enhancements, at least not at energies accessible to *ACE* SIS. (But in all three events, Fe/O increases with energy above ∼40 MeV nucleon^{-1}.) It is perhaps relevant that these events occurred late in the solar cycle, after the general level of flare activity had significantly decreased.

Overall, in Table 2 and Figure 10, 33 of the 38 GLEs (that is, 87%) have measured Fe/O at more than twice the nominal coronal value at energies of ∼40 MeV nucleon^{-1} or higher. By comparison, only 14 of the 30 non-GLEs in Table 1 (47%) exhibit this characteristic. Thus, high-energy Fe/O enhancements are significantly more common among GLEs. This is another important challenge for alternative hypotheses and future SEP modeling efforts.

3.4. *Event Duration at High Energies*

Tsurutani & Lin (1985) noted that quasi-perpendicular shocks at 1 AU produce "spikes" in proton time-intensity profiles, whereas quasi-parallel shocks tended to produce profiles with longer lasting "plateaus." Similar behavior might also be expected among the high-energy particles produced near the Sun. In a quasi-parallel configuration, the shock can remain in contact with a given group of magnetic flux tubes for an extended period of time, producing a time-intensity profile that is comparatively flat. In the quasi-perpendicular case, on the other hand, the shock generally crosses quickly over the group of flux tubes, resulting in a more impulsive-looking "spike" in the profile. These time-structure effects would be less apparent at low energies, which can be produced over a broader extent of the shock front.

A suggestion of this behavior is seen in Figure 11, which shows the *GOES* proton time lines for the events of Figure 1. Apart from normalization, the shapes of the >10 MeV profiles are similar in the two events. But this is not the case at the higher energies that are more relevant to our hypothesis about near-Sun shock geometry. Whereas the >50 and >100 MeV protons are constant for nearly a day in the (quasi-parallel) April event, they decline sharply within a few hours after the peak in the (quasi-perpendicular) August event. (It is important to remember that the CMEs and flare locations in these two events are nearly identical; the difference in the high-energy proton profiles therefore cannot be casually dismissed as a consequence of "connection.") In fact, the high-energy profiles in the August event are nearly classic examples of a short-lived accelerator at the Sun, followed by diffusion to 1 AU.

[17] *SAMPEX* measured $\langle Q_{Fe} \rangle = 12 \pm 1$ and $Q_O = 6.6 \pm 0.3$ above ∼25 MeV nucleon^{-1} in this event (Labrador et al. 2003). These relatively low charge states may suggest a paucity of flare remnants in the seed population for this particular event.

TABLE 2

HIGH-ENERGY Fe/O FROM *IMP8* IN GROUND LEVEL EVENTS, SOLAR CYCLES 21 AND 22

GLE No.[a]	Start Date (UT)	Start Time (UT)	Source Location[b]	Ion Accumulation Time (hr)	Number of Iron Ions[c] (47–80 MeV nucleon^{-1})	Number of Oxygen Ions (43–86 MeV nucleon^{-1})	Fe/O/0.134[d] (47–80 MeV nucleon^{-1})
27[e]	1976 Apr 30	20:00	S08, W46	12.0	9.0	13	$9.0^{+5.4}_{-3.6}$
28	1977 Sep 19	10:00	N08, W57	30.0	39.0	38	11.0 ± 2.2
29	1977 Sep 24	06:00	N10, W120	27.0	123.0	125	9.2 ± 1.0
30	1977 Nov 22	10:00	N24, W40	26.0	28.5	45	6.7 ± 1.5
31	1978 May 7	03:00	N23, W72	16.0	7.5	16	$4.9^{+3.3}_{-2.1}$
32	1978 Sep 23	10:00	N35, W50	30.0	22.5	28	$8.9^{+2.9}_{-2.3}$
34	1981 Apr 10	16:00	N07, W36	24.0	3.0	4	10^{+13}_{-6}
35	1981 May 10	07:00	N03, W75	24.0	1.5	3	8^{+19}_{-7}
36[f]	1981 Oct 12	06:00	S18, E31	50.0	4	13	$4.1^{+3.2}_{-1.9}$
37	1982 Nov 26	02:00	S12, W87	12.0	4.5	8	$6.2^{+6.0}_{-3.3}$
38	1982 Dec 7	23:00	S19, W86	32.0	19.5	39	$5.4^{+1.9}_{-1.5}$
39	1984 Feb 16	09:00	S, W130	24.0	10.5	18	$6.3^{+3.4}_{-2.3}$
40	1989 Jul 25	08:00	N26, W85	24.0	3.0	1	22^{+110}_{-16}
41	1989 Aug 16	01:00	S15, W85	26.0	33.0	87	4.1 ± 0.9
42[f]	1989 Sep 29	11:00	S24, W105	72.0	22	77	3.3 ± 0.7
43[f]	1989 Oct 19	12:00	S25, E09	24.0	48	138	3.6 ± 0.6
44[f]	1989 Oct 22	18:00	S27, W32	36.0	2	19	$1.2^{+1.6}_{-0.8}$
45[f]	1989 Oct 24	18:00	S29, W57	50.0	27	77	3.9 ± 0.8
46	1989 Nov 15	06:00	N11, W28	17.0	7.5	16	$5.0^{+3.4}_{-2.4}$
47	1990 May 21	22:00	N34, W37	53.0	33.0	21	15.5 ± 3.5
48	1990 May 24	20:00	N36, W76	36.0	28.5	34	8.9 ± 2.0
49	1990 May 26	21:00	N35, W103	32.0	9.0	15	$8.2^{+4.9}_{-3.2}$
50	1990 May 28	04:00	N35, W120	84.0	10.5	5	24^{+18}_{-10}
52	1991 Jun 15	08:00	N36, W70	42.0	1.5	52	$0.4^{+0.9}_{-0.3}$
53	1992 Jun 25	20:00	N09, W69	41.0	24.0	99	2.5 ± 0.6

[a] From the catalog of ground-level events provided by the Australian Antarctic Data Center at http://aadc-maps.aad.gov.au/aadc/gle/index.cfm. Three GLEs have been omitted from this table: No. 33 (1979 August 21; Fe/O dominated by the decay phase of a previous event); No. 51 (1991 June 11; no *IMP8* data coverage); and No. 54 (1992 November 2; no *IMP8* data coverage in the first 12 hr).

[b] From Shea & Smart (1993).

[c] Numbers have been corrected for a priority scheme that records only two-thirds of the Fe ions registered in this energy bin. No priority correction is required for the oxygen ions, which come to rest at deeper levels in the detector stack.

[d] Normalized to the nominal coronal value (0.134; Reames 1995) and corrected for priority scheme, Galactic and anomalous cosmic-ray oxygen backgrounds, and the difference in oxygen and iron energy intervals.

[e] Combined data from nearly identical instruments on *IMP8* and *IMP7*.

[f] These results are from higher energies: Fe ions at 97–175 MeV nucleon^{-1}, O ions at 86–180 MeV nucleon^{-1}, and Fe/O ratio corrected to the common interval 97–175 MeV nucleon^{-1}. Because of the very high count rates in these events, the priority corrections required to evaluate Fe/O at 47–80 MeV nucleon^{-1} are larger than usual. We quote these higher energy values, for which no priority corrections are needed. Fe/O increases with energy in the 1981 October 12 and 1989 September 29 events (Tylka & Dietrich 1999).

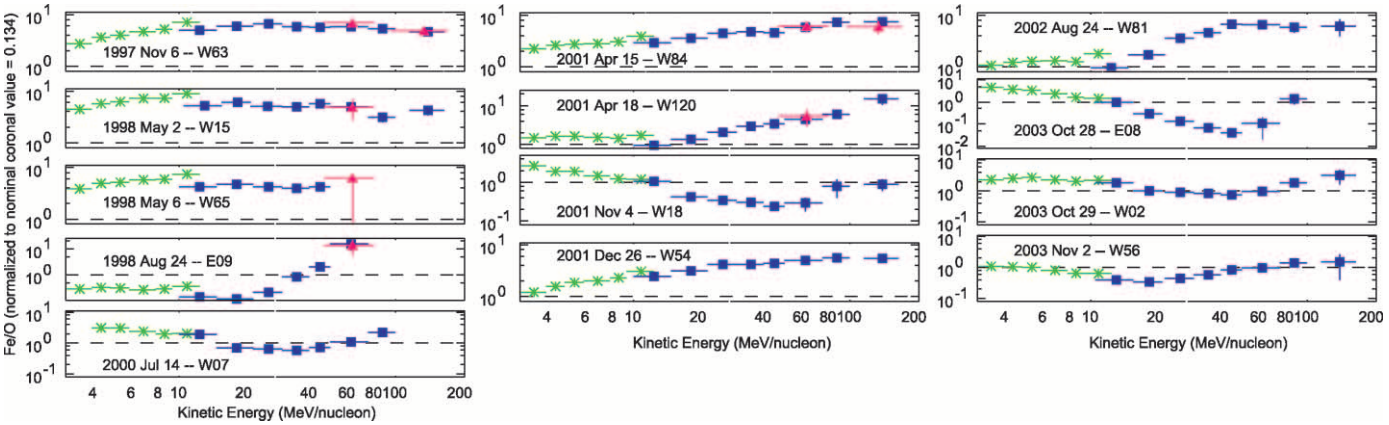

FIG. 10.—Measurements of event-integrated Fe/O (normalized to the nominal coronal value) from *Wind* LEMT (*green asterisks*), *ACE* SIS (*blue squares*), and *IMP8* CRNE (*red triangles*) at ~3–200 MeV nucleon^{-1} in the 13 ground-level events of 1997–2003. Date and solar-source longitude is noted in each panel. The *y*-axis differs from panel to panel; the dashed line marks the nominal value. Routine data collection from *IMP8* terminated in 2001 October. Note that SIS measures stopping iron up to 168 MeV nucleon^{-1} but oxygen only up to 89.3 MeV nucleon^{-1}. Accordingly, the next to highest energy SIS data points (at 75–100 MeV nucleon^{-1}) involve a modest correction, derived from a fit to the oxygen spectrum. The highest energy SIS data points (at 117–168 MeV nucleon^{-1}) rely totally on the extrapolations of the fitted oxygen spectra and should therefore be accepted with appropriate caution.

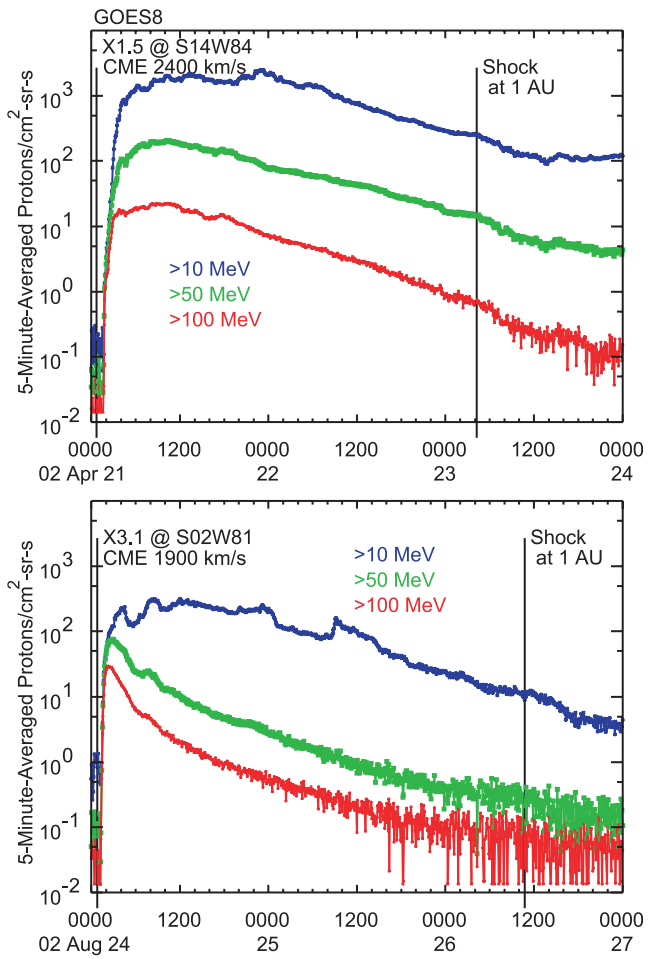

FIG. 11.—Time lines of 5 minute averaged integral proton intensities from *GOES-8* for the 2002 April 21 (*top*) and 2002 August 24 (*bottom*) events. Intensities are shown for >10 (*blue*), >50 (*green*), and >100 MeV (*red*). At >10 MeV, the events are similar, except for normalization. But at higher energies the durations of the events are markedly different. The peak intensity at >100 MeV is greater in the August event. Note that at these energies, there are no significant increases associated with the shock arrival at Earth.

Figure 12 looks for a similar effect in the other events. We identified 26 events in which the hourly averaged intensity of >100 MeV protons on *GOES* exceeded 1.0 proton cm^{-2} sr^{-1} s^{-1}. This relatively high threshold requirement discriminates against far eastern events, whose profiles are extended for other reasons (Cane et al. 1988; Reames et al. 1996). The duration of the >100 MeV protons was defined as lasting from onset until the decay-phase intensity had fallen to 10% of the event maximum. The shapes of time profiles are also affected by source location, so filled symbols distinguish events in which the associated flare longitude was between W30° and W90°. There is a reasonably clear anticorrelation between this duration and enhanced Fe/O. This is as we would expect if long-lasting events were quasi-parallel while events with enhanced Fe/O were quasi-perpendicular.

In summary, if enhanced Fe/O at high energies is a signature of a quasi-perpendicular shock while near the Sun, then we should expect (1) an anticorrelation between high-energy Fe/O and event size; (2) an anticorrelation between high-energy Fe/O and spectral steepening; (3) enhanced high-energy Fe/O in GLEs;

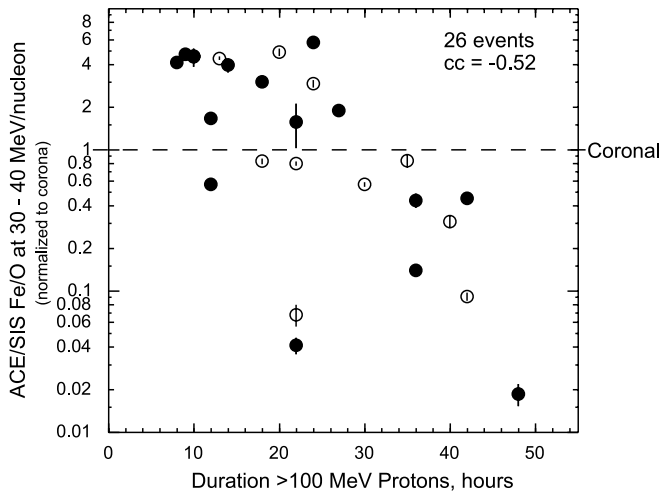

FIG. 12.—Correlation of event-integrated Fe/O at 30–40 MeV nucleon^{-1} vs. the duration of *GOES* protons above 100 MeV. The duration was measured from onset until the intensity had decayed to 10% of its peak value. Filled circles represent events with associated flare longitudes at W30°–W90°.

and (4) an anticorrelation between high-energy Fe/O and the duration of the event at high energies. All of these expectations are fulfilled, both for the archetypal events in Figure 1 and for our statistical study of the largest SEP events of 1997–2003. Although these correlation studies may not be sufficient to prove our hypothesis about the role of near-Sun shock geometry, they certainly demonstrate that the notion merits further consideration.

4. AN ALTERNATIVE HYPOTHESIS: A DIRECT FLARE COMPONENT AT HIGH ENERGIES

The dominant role of fast, CME-driven shocks in producing particles below ~10 MeV nucleon^{-1} is not in question. We have hypothesized that enhanced Fe/O at even higher energies also come from a shock, but operating on a seed population containing flare suprathermals. An alternative hypothesis would be two distinct acceleration mechanisms operative in the same event, with a shock producing the lower energy particles while a flare alone directly generates most of the higher energy particles. Although this two-component model cannot explain the Fe-rich IPS events, it is nevertheless a logical possibility for the SEP events. Moreover, both hypotheses imply that the high-energy particles should carry the compositional signatures of flare-acceleration. It is thus difficult to distinguish between the hypotheses using *only* the composition data. We therefore now consider three other lines of evidence that address this issue.

4.1. *Longitude Distribution*

First, classic flare-accelerated "impulsive" events, in which ^{3}He/^{4}He at a few MeV nucleon^{-1} exceeds 10%, are clustered around W50°, with ~85% of the associated flares located between W30° and W80°. (See, for example, Fig. 2.3 of Reames [1999]. A comparable distribution is also found in a list of *ACE* impulsive events [Mason et al. 2002].) According to Reames (1999), most of this spread in the connection longitude results from variation in solar-wind speed, with the remainder due to random walk of the magnetic field lines (Mazur et al. 2000; Giacalone et al. 2000).

Figure 13 plots event-integrated Fe/O at 30–40 MeV nucleon^{-1} versus the longitude of the associated flare (Cane et al. 2002, 2003) for the SEP events in this study. Only about one-third of the Fe-enhanced events in Figure 13 fall within this "well-connected" longitude range. The associated flares in the other events are at longitudes ranging from E16° to W140°. The very broad longitude distribution in Figure 13 is incompatible with the direct-flare hypothesis.[18] Of course, the larger Fe-rich events tend to be found near well-connected longitudes. However, that is not surprising: at these longitudes, the strongest parts of the shock are more likely to intercept the Sun-Earth field line while still near the Sun.

Figure 14 shows a particularly striking example, the 1999 January 20 event. The >30 MeV proton fluence in this event was slightly too small (~1.7×10^5 cm^{-2} sr^{-1}) to be included in our SEP survey. Mason et al. (1999b) have previously identified this event as an example of enhanced ^{3}He/^{4}He due to flare remnants reaccelerated by a CME-driven shock. According to Cane et al.

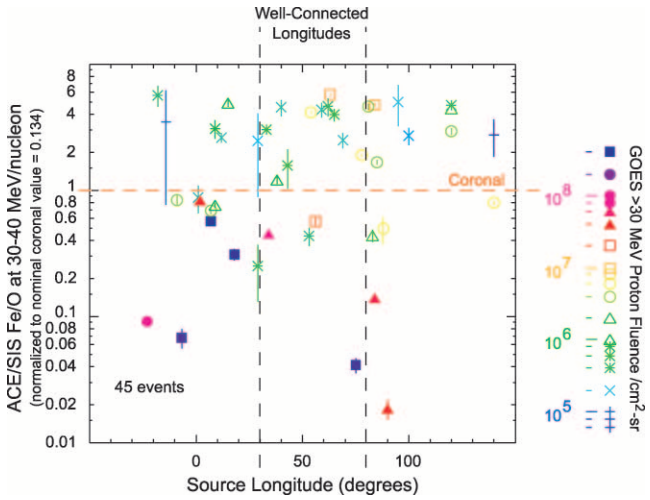

FIG. 13.—Correlation of event-integrated Fe/O at 30–40 MeV nucleon^{-1} vs. solar longitude of the source. Source longitudes are from Cane et al. (2002, 2003) or (for more recent events, not included in their lists) from *Solar Geophysical Data* or the *GOES* solar proton event list at http://umbra.nascom.nasa.gov/SEP/seps.html. The color and symbol shape indicate the event-integrated proton fluence above 30 MeV from *GOES*, as shown in the legend at the right. The vertical dashed lines demarcate "well-connected" longitudes at which impulsive (flare-accelerated) SEP events are generally observed (see text). For completeness, the plot also contains four additional events from Cane et al. (2002) (1998 May 9 at W100°, 2000 June 6 at E14°, and 2001 May 7 at W140°) and Gopalswamy (2003) (2001 October 19 at W29°) for which *ACE* SIS was able to measure Fe/O at 30–40 MeV nucleon^{-1}, even though the >30-MeV proton fluence fell slightly below that of our event selection criterion.

(2002), the source region for this event was at E95°, behind the east limb.[19] At ~1 MeV nucleon^{-1}, Fe/C is suppressed relative to the corona. But Fe has a harder power-law spectrum than C—the same sort of spectral difference found at high energies in the 2002 August 24 event and other western GLEs (Tylka et al. 2002). This spectral difference causes the Fe/C ratio to increase with energy, attaining values at ~10–20 MeV nucleon^{-1} that are nearly characteristic of flare-accelerated particles.

The *IMP8* CRNE also reported enhanced Fe/O above 40 MeV nucleon^{-1} in two other eastern events (Tylka & Dietrich 1999),

[18] This conclusion disagrees with von Rosenvinge et al. (2001). That study was based on fewer events, and the *ACE* SIS Fe/O values were integrated over 12–60 MeV nucleon^{-1}. The lower integration-threshold may have obscured the behavior at the higher energies.

[19] *GOES* reported an M5.2 X-ray flare in association with this event. *Yohkoh* placed the location of this flare at N29°, E87° (J. Mariska 2004, private communication). *SOHO* was not operational at the time, but the Mauna Loa Mk4 coronagraph observed CME activity already in progress on the northeast limb when it began observations at 1758 UT (J. Burkepile 2004, private communication). *GOES* first observed the associated X-ray flare at 1905 UT. Palehua and Sagamore Hill stations reported metric type II emission at 1914–1923 UT (*Solar Geophysical Data*), and *Wind* Waves registered strong DH type II radio emission from 1918–1946 UT (http://lep694.gsfc.nasa.gov/waves/waves.html). However, particle instruments on *Wind* and *ACE* did not observe increases in ~20 MeV nucleon^{-1} protons and heavy ions until ~2200 UT. *Wind* LEMT, which monitors arrival directions covering nearly the whole sky, confirmed that the particles were flowing outward from the direction of the Sun. The long delay in the particle onsets is qualitatively consistent with shock propagation from an eastern source location to the field line connected to Earth. Moreover, there are no other plausible candidate sources for this SEP event. *GOES* did not report another X-ray flare (C5.1 at N19°, W26°) until 0424 UT on January 21, too late to be related to the observed particle increase. According to Solar Geophysical Data, there was a small, faint ("SF") Hα flare at S24°, W25° at 2123–2133 UT. Although this time is not incompatible with the SEP onset, it is unlikely that such a minor flare could produce the observed energetic particles, which included >100 MeV protons. There also appears to have been no significant radio emission associated with this minor flare, which would also be highly unlikely for an SEP producer (Cliver et al. 2004).

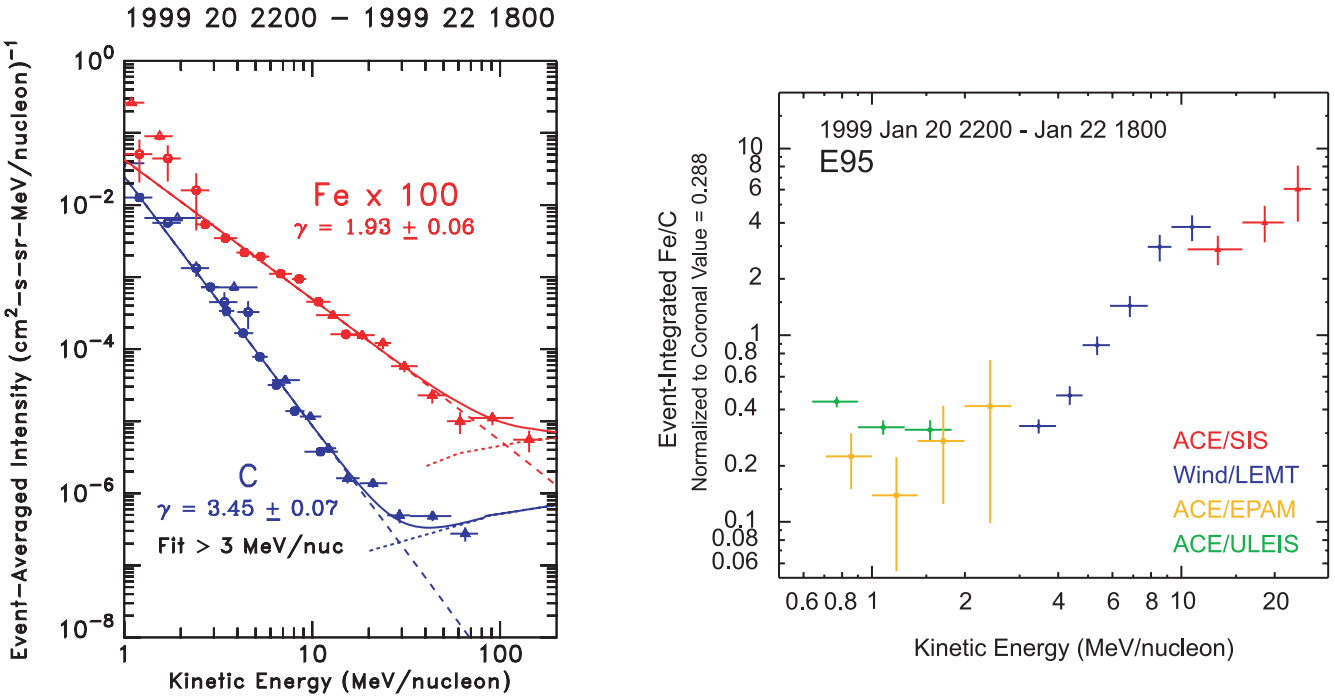

FIG. 14.—Event-averaged energy spectra (*left panel*) for C (*blue*) and Fe (*red*; multiplied by 100) and Fe/C vs. energy (*right panel*) in the east-limb solar particle event of 1999 January 20 event. In the left panel, the short-dashed curves in the lower right show the Galactic cosmic-ray background. Also shown are power-law fits to the spectra above 3 MeV nucleon^{-1}, along with the fitted values of the power-law spectral index. Colors distinguish the instruments used in the right panel. Fe has a harder spectrum than C, causing Fe/C to increase with energy. In this relatively small event, we have compared Fe to C, rather than O, so as to avoid potential complications due to anomalous cosmic rays.

1979 August 19 (at E90°, according to Cane et al. 1986) and 1978 April 28 (at E38°). The 1999 January 20 event is therefore rare but not unique.

Thus, high-energy Fe/O enhancements are found in association with flares ranging across the whole Sun, from behind the east limb to well beyond the west limb. It is difficult to see how this fact can be reconciled with a direct flare component. However, a broad longitude distribution arises naturally in the context of CME-driven shocks.

The broad longitude distribution in Figure 13 suggests that in most events, the flare suprathermal seed particles are remnants from previous flare activity, rather than from the event's associated flare. The latter may also contribute seed particles in events with flares at well-connected longitudes. In fact, if open field lines connect the flare site to the shock front, these "fresh" (as opposed to "remnant") flare suprathermals might explain the comparatively high proportion of Fe-rich events at well-connected longitudes. However, such a conclusion requires better event statistics and more thorough analysis of individual events.

4.2. *Spectral Characteristics*

Second, the observed spectra provide no support for the direct-flare hypothesis. According to that hypothesis, the flare is more prolific than the shock at producing the highest energy particles. From this superposition of two distinct accelerators, one should therefore expect spectra that harden with increasing energy, as illustrated schematically in Figure 15. (Of course, it is possible that the relative strengths and spectral shapes of the two components could be such that they minimize the appearance of a spectral break. But if the two components truly are independent, there is no reason to believe that such an arrangement should generally be the case.) This spectral hardening should be particularly acute in event-integrated spectra, where (according to this alternative hypothesis) the highest energy particles are produced by the flare for a brief time, while the shock continues to pump up the softer, lower end of the spectrum over an extended period.

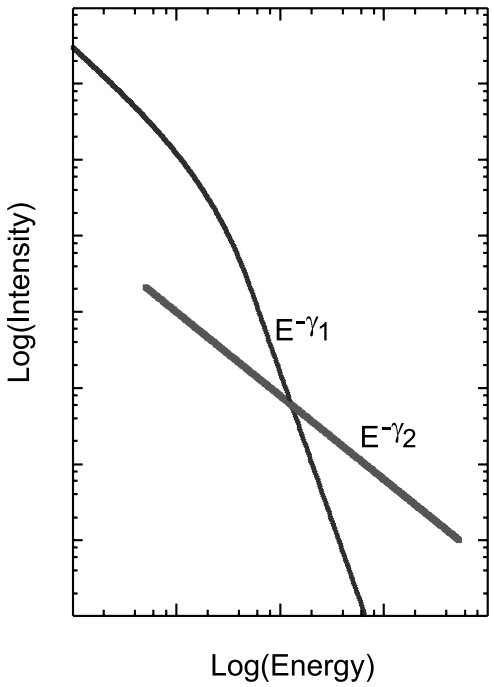

FIG. 15.—Schematic representation of energy spectra we would expect if two distinct acceleration mechanisms were operative, with the second being more effective at producing high-energy particles. In this case, we would find $\gamma_2 - \gamma_1 < 0$.

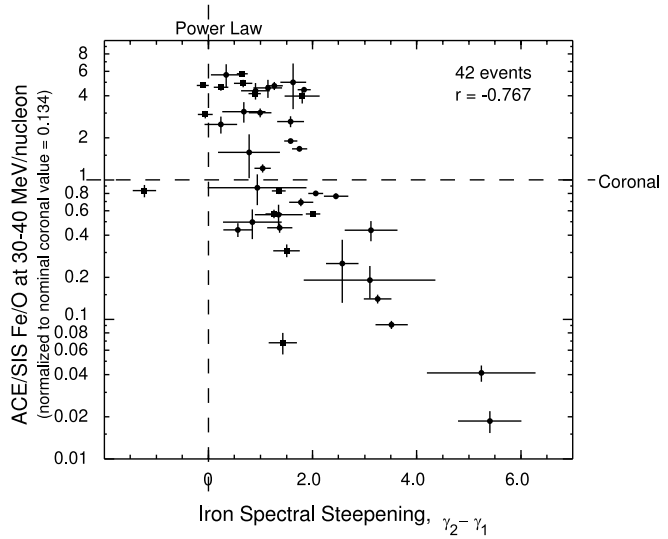

FIG. 16.—Correlation of event-integrated Fe/O at 30–40 MeV nucleon^{-1} vs. spectral steepening of the iron spectrum, as described in the text. The calculated correlation coefficient (−0.767) excludes the one event (1998 August 24) in which $\gamma_2 - \gamma_1$ is significantly less than zero.

If enhanced Fe/O at high energies signals the presence of particles directly accelerated by a flare, then this spectral hardening should be detectable in both oxygen and iron. As already noted, there is no evidence for spectral hardening in the oxygen spectra (see Fig. 9). Figure 16 shows the same study, but for iron. As before, we fit the Fe spectrum to two independent power laws, one ($E^{-\gamma_1}$) at 3–10 MeV nucleon^{-1} and the other ($E^{-\gamma_2}$) at 21–100 MeV nucleon^{-1}. (We used 21, instead of 30, MeV nucleon^{-1}, as the lower boundary of this second interval so as to ensure that there are at least two energy bins in which *ACE* SIS measured SEP Fe, even in events in which the Fe spectrum is very steep at high energies.) The values of γ_1 and γ_2 are listed in columns (11) and (12) of Table 1.

There is only one event (1998 August 24) in our SEP survey in which the event-integrated Fe spectrum actually looks like Figure 15, with $\gamma_2 - \gamma_1$ significantly less than zero. The unusual temporal evolution of the spectral shape in this particular event has been discussed previously (Tylka et al. 2000). However, this event is not especially convincing as a candidate for a direct flare component, since the associated flare was at E08° (Cane et al. 2002).

Events with clear hardening in the event-integrated Fe spectrum appear to be rare. We found only one other example, 2000 June 6, among events whose >30 MeV proton fluences were slightly too small for inclusion in our SEP survey. The associated flare in this event was also east of central meridian, at E14° (Cane et al. 2002), making it another unlikely candidate for a direct flare component. It is intriguing that in both cases, this rare behavior occurred in events in which the source region was slightly east of central meridian. This fact may suggest an interesting and distinctive evolution in shock geometry in events like these.

4.3. *Timing Studies*

Finally, timing studies directly address the relative roles of flares and CME-driven shocks in producing the energetic particles observed at Earth. Previous timing studies (e.g., Kahler 1994; Debrunner et al. 1997) have favored CME-driven shocks as the accelerators. Recent work, which has benefitted from new instrumentation with unprecedented sensitivity and timing resolution, has confirmed these earlier conclusions. Timing studies are beyond the scope of this paper, so we simply take note of these recently reported results:

1. Falcone et al. (2003) studied >5 GeV protons detected by the Milagrito air shower array in the 1997 November 6 GLE. On the basis of the ∼20 minute delay between the gamma-ray emission reported by *Yohkoh* (Yoshimori et al. 2002) and the first arrival of protons at Earth, they conclude that "it is not possible that the solar flare particles as manifested in the gamma-ray flare are responsible for the ground-level event."

2. Bieber et al. (2004) modeled time-intensity profiles and arrival-direction anisotropies recorded by the "Spaceship Earth" worldwide neutron monitor network on 2001 April 15, the largest GLE in 1997–2004 (Lockwood et al. 2002; Poirier & D'Andrea 2002). They determined the injection time of ∼GeV particles at the Sun to within 1 minute uncertainty. They wrote: "Since the CME release and flare onset both preceded the particle injection onset, acceleration in the flare or by a CME shock are both possible sources for the GeV solar particles observed on Easter 2001. Nonetheless, the onset timing would tend to favor shock acceleration, because (1) the particle injection onset is closer in time to the CME liftoff than the flare onset (∼15 vs. 31 minutes), and (2) the particle injection onset is accompanied by shock-associated radio signatures." They concluded that their results "are consistent with the hypothesis that solar particles were accelerated to GeV energies (in this event) by a CME-driven shock."

3. Tylka et al. (2003) combined electron, proton, and ion data from *IMP8*, *Wind*, *ACE*, and neutron monitors. They analyzed velocity dispersion in the first arrival at Earth using the standard "onset time versus $1/\beta$" method (Lin et al. 1981; Reames et al. 1985; Krucker et al. 1999). They determined the solar particle release times to within ∼1 minute uncertainty. In the 1997 November 6 and 2001 April 15 GLEs (both of which also have enhanced Fe/O above 10 MeV nucleon^{-1}), they found that the earliest departure of energetic particles from the Sun occurred ∼25 and ∼7 minutes, respectively, after the start of the 4–7 MeV gamma-ray emission recorded by *Yohkoh*. By these times, the gamma-ray emission was either finished or well into its decay phase. They also examined the timing in two classic impulsive events, 2000 May 1 (Reames 2000; Mason et al. 2002) and 2001 April 14 (Tylka et al. 2002). In contrast to the GLEs, the particle release in the impulsive events was simultaneous to within 1 minute with the peak of the hard X-rays, the highest energy photons observed in those events.

4. Mewaldt et al. (2003b) examined the velocity dispersion of 6–88 MeV nucleon^{-1} $Z \geq 6$ ions in 11 events observed by *ACE* SIS. Except for three impulsive events and the 1998 May 6 GLE,[20] they inferred that the particle release came when the associated CMEs were more than 2 solar radii above the photosphere. The authors did not discuss the timing relative to flare activity, but these inferred altitudes would tend to favor origin from the CME-driven shock.

Thus, although these timing studies start with different data sets, different analysis techniques, and different assumptions about the underlying particle transport, they all conclude that the release of particles into interplanetary space—even at the highest

[20] In terms of proton fluence above 100 MeV, the 1998 May 6 event is the smallest GLE to date in cycle 23. Tylka et al. (2003) also examined this event and concluded that the timing analysis could not distinguish between flare and shock origin in this particular case.

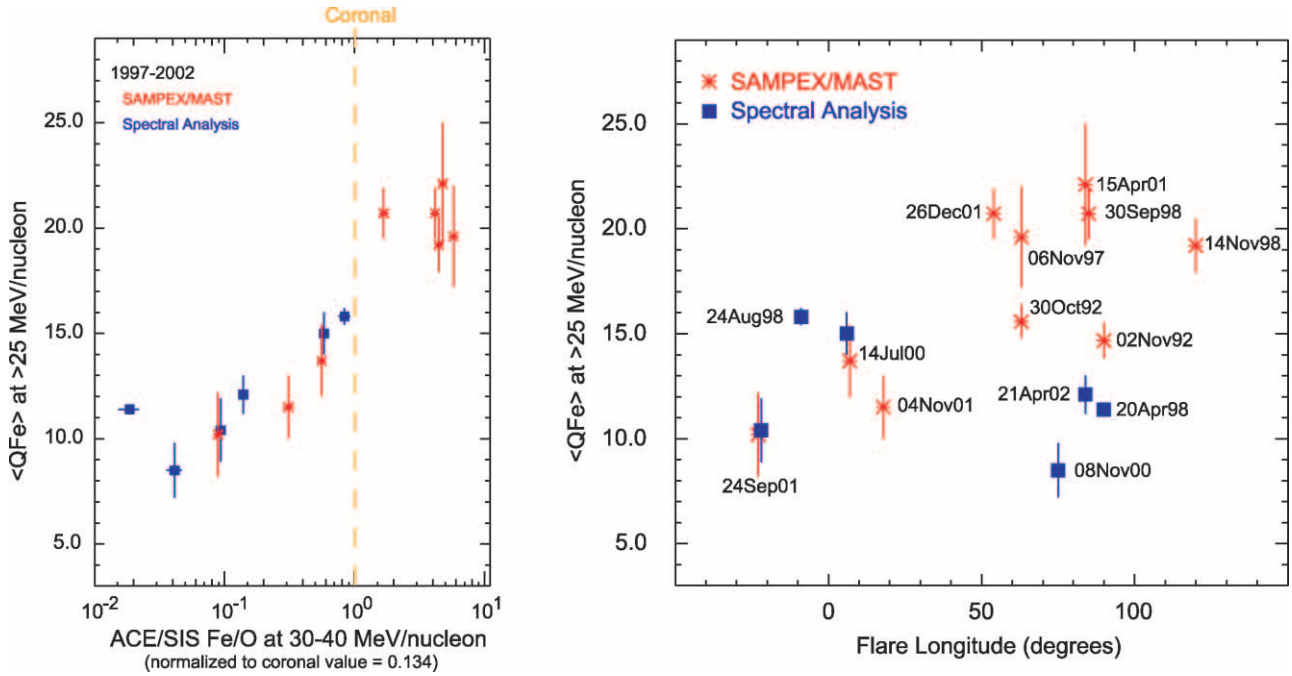

FIG. 17.—Measurements of $\langle Q_{Fe} \rangle$ from the Mass Spectrometer Telescope (Cook et al. 1993) on *SAMPEX* (*red asterisks*) at $\gtrsim$25 MeV nucleon^{-1} (Leske et al. 1995, 2001; Labrador et al. 2003) and from spectral analyses (Tylka et al. 2000, 2001) at comparable energies (*blue filled squares*) plotted vs. *ACE* SIS Fe/O at 30–40 MeV nucleon^{-1} (*left panel*) and the longitude of the event's associated flare (*right panel*). Two events (2000 July 14 and 2001 September 24) have been measured by both methods.

energies—favors origin from the CME-driven shock, rather than the associated flare.[21]

In summary, a direct flare component is a reasonable a priori hypothesis, given only the high-energy composition data. But three independent lines of argument—the longitude distribution of Fe-rich events, their spectral characteristics, and timing studies—pose challenges for this hypothesis. These challenges should not be dismissed without careful and detailed consideration. But all of these observations are consistent with acceleration by a CME-driven shock.

4.4. *Comment on High-Energy* Fe *Charge State Measurements*

Measurements of the mean ionic charge state of Fe ($\langle Q_{Fe} \rangle$) at high energies also bear on the question of a direct flare component (Tylka et al. 1995). Figure 17 shows $\langle Q_{Fe} \rangle$ measurements at $\sim$25–100 MeV nucleon^{-1}, as deduced from analysis of geomagnetic penetration observed by the *SAMPEX* (Leske et al. 1995, 2001; Labrador et al. 2003). Also plotted in Figure 17 are additional high-energy $\langle Q_{Fe} \rangle$ values, as inferred from analysis of the Q/A-dependent exponential rollovers at comparable energies (Tylka et al. 2000, 2001). The two methods agree well in the two events (2000 July 14 and 2001 September 24) in which both methods were applicable. But, in general, the two methods are complementary: the spectral analysis relies on steeply falling Fe spectra that generally yield too few high-energy Fe ions for reliable detection by *SAMPEX*, whereas the hard-spectra events most easily accessible to *SAMPEX* generally do not exhibit exponential rollovers.

The left panel of Figure 17 shows the high-energy $\langle Q_{Fe} \rangle$ plotted versus the *ACE* SIS Fe/O at 30–40 MeV nucleon^{-1}. This clear correlation has been noted before (e.g., Leske et al. 2001). We note in passing that this correlation is a challenge for models that seek to explain the increase in Fe/O with energy in terms of "smoothed shocks" (Eichler 1979; see also the discussion in Tylka et al. 2002). Moreover, in those events with the largest Fe/O values, the Q/A difference between oxygen and iron is relatively small, also making it difficult to account for the enhancement through an unusual rigidity dependence in near-shock scattering conditions, as suggested by Cohen et al. 2003.

The right panel of Figure 17 shows $\langle Q_{Fe} \rangle$ plotted versus the longitude of the associated flare. Given only the *SAMPEX* results, one might be tempted to infer a significant correlation between $\langle Q_{Fe} \rangle$ and the flare longitude. Such a correlation might be interpreted as evidence for the direct-flare hypothesis. However, the additional $\langle Q_{Fe} \rangle$ values from the spectral analysis considerably weaken the apparent correlation. Events with $\langle Q_{Fe} \rangle \sim 10$–12 span longitudes from E23° to W90°. Near nominally well-connected longitudes, $\langle Q_{Fe} \rangle$ values range from $\sim$10 to $\sim$22.

As seen in Figure 17, the easternmost event for which *SAMPEX* reports $\langle Q_{Fe} \rangle \gtrsim 16$ is at W54°. But as shown in Figure 13, there are eight events with enhanced Fe/O where the associated flare is even farther east. Figure 18 clarifies why *SAMPEX* has not reported $\langle Q_{Fe} \rangle$ for these events. The figure plots the event-integrated Fe fluences observed by *ACE* SIS at 26–118 MeV nucleon^{-1} (roughly the same energy range as covered by the *SAMPEX* data in Fig. 17) versus the associated flare's longitude. *SAMPEX* apparently can extract an $\langle Q_{Fe} \rangle$ measurement only when the high-energy Fe fluence exceeds $\sim$100 Fe cm^{-2} sr^{-1}. Fe/O-enhanced events outside the well-connected longitudes simply produced too few high-energy Fe ions for measurement by *SAMPEX*. Thus, there is a significant observational limitation in

[21] For completeness, we also note a statistical study of near-relativistic electron events from *ACE* EPAM (Haggerty & Roelof 2002). This study is not immediately relevant to this paper, since it examined only electrons and made no attempt to classify the events on the basis of their ionic characteristics. Nevertheless, the authors concluded that, on average, >300 keV electrons are injected onto the Sun-Earth field line $\sim$10 minutes after the start of electromagnetic emissions. Simnett et al. (2002) compared the electron release times to *SOHO* CME observations and suggested "that the near relativistic electrons observed by *ACE* EPAM are accelerated by the shock ... and released at a radial distance around 2–3 solar radii (from the Sun center)." However, see Kahler et al. (2005) for a critique of this study.

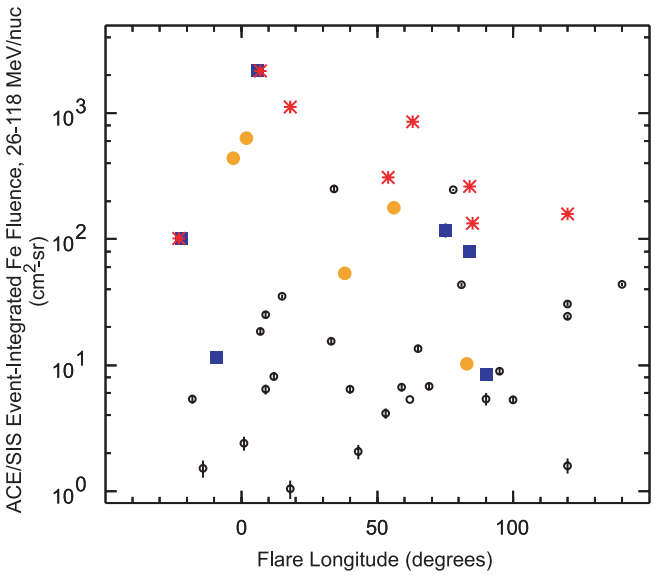

FIG. 18.—Event-integrated Fe-fluence at 26–118 MeV nucleon^{-1} from *ACE* SIS plotted vs. longitude of the associated flare. Red asterisks represent events in which there are $\langle Q_{Fe} \rangle$ measurements at roughly this same energy from *SAMPEX* (Leske et al. 2001; Labrador et al. 2003). Filled blue squares represent events in which $\langle Q_{Fe} \rangle$ could be inferred from spectral analyses, as discussed in Tylka et al. (2000, 2001). (Two events were measured by both methods.) Filled gold circles represent the events of 2003 October–November for which charge state studies have not yet been published. Small black circles represent events for which there is presently no information on $\langle Q_{Fe} \rangle$ at high energies.

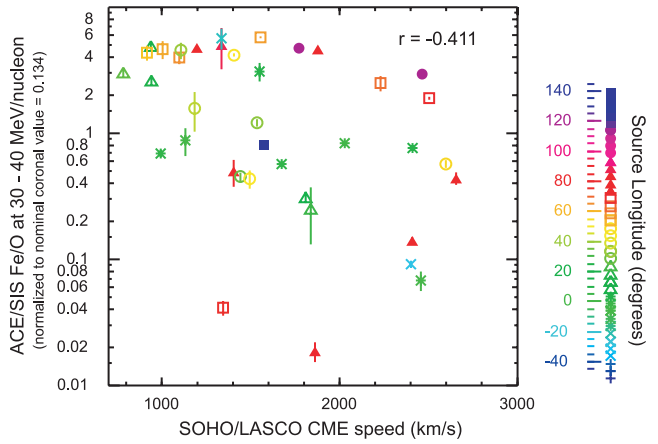

FIG. 19.—Correlation of event-integrated Fe/O at 30–40 MeV nucleon^{-1} for the events of Table 1 vs. the measured speeds of the associated CMEs, as given by http://cdaw.gsfc.nasa.gov/CME_list. The correlation coefficient between these variables is −0.411. Color and symbol shape indicate the source longitude, as indicated by the legend at the right. The CME speeds have not been corrected for possible projection effects.

the events accessible to *SAMPEX*. It is accordingly premature to conclude that high $\langle Q_{Fe} \rangle$ events are found *only* at well-connected longitudes, as the direct-flare hypothesis would suggest.

5. DISCUSSION

In conclusion, we have proposed that the interplay of two variable factors—shock geometry and seed population—provide a framework for understanding the overall variability at high energies in large SEP events. The hypothesis requires a compound seed population, comprising at least solar-wind and flare suprathermals. Shock geometry—by setting the energy at which effective injection occurs—determines which of these components should dominate in providing the seeds for high-energy SEPs. We have shown that our hypothesis appears consistent with recent observations of traveling interplanetary shocks near 1 AU, in which we have direct information about both the seed population and shock geometry. For SEPs, our hypothesis provides a unified accounting of observed correlations among high-energy Fe/O, event size, spectral characteristics, the presence of GeV particles, and event duration at high energies. Although these correlation studies cannot be construed as proof of our hypothesis, they certainly confirm its viability. Moreover, one could probably construct an alternative scenario to explain any one of the observed correlations. But the strength of our hypothesis is that it simultaneously addresses all of them. Our hypothesis is also attractive in that, rather than invoking two distinct acceleration mechanisms at high energies, it exploits known parameter variation that is inherent in shock acceleration. Indeed, given the substantial body of theoretical work on the likely importance of geometry (that is, θ_{Bn}) in shock acceleration, we should probably be surprised if we could not find some reflection of it in the SEP observations.

The synergistic roles of shock angle and seed population have also recently been considered in another context: Meziane et al. (2002) presented a statistical study of 216 energetic ion events observed by the *Wind* spacecraft just upstream of Earth's bow shock. The classified their events according to both the value of θ_{Bn} and the presence or absence of a preexisting energetic seed population above 50 keV. They observed event-to-event variability in spectral character, qualitatively similar to that displayed in our Figure 8, albeit at much lower energies. In particular, they found that for quasi-parallel configurations, the spectra showed a roughly exponential rollover with at cutoff at ~200–300 keV, in agreement with Lee's (1982) self-consistent theory of diffusive shock-acceleration at the bow shock. This cutoff was independent of whether or not the preexisting energetic seed population was present. The observed spectra showed the same behavior at quasi-perpendicular shocks when the preexisting energetic seed population was absent. But when the preexisting energetic seed population was present *and* the shock was quasi-perpendicular, the spectra showed a power-law extension up to ~2 MeV. The authors attributed these higher energy ions to shock-drift acceleration. Of course, the small size of Earth's bow shock limits shock acceleration in ways for which there are no corresponding factors in SEP events. One must therefore be cautious in drawing analogies between these two cases. But it is nevertheless intriguing that the bow shock shows a range of spectral morphology qualitatively similar to what we see in the high-energy SEPs, and that the apparent origin of that variability hinges on the same factors that we have identified in this study.

Shock speed is an important factor in SEP production, although it does not fully account for SEP variability (Kahler 1999). One might nevertheless wonder whether event-to-event variability in shock speed alone, without any appeal to shock geometry, might be sufficient to account for higher injection thresholds that appear to preferentially select flare suprathermals in some events. To address this question, Figure 19 plots the high-energy Fe/O versus the measured CME speeds for our SEP events. There is a modest anticorrelation between these observables, with a larger proportion of events having enhanced Fe/O at lower speeds. The enhanced Fe/O events are certainly not primarily at the highest CME speeds, which one would expect if shock speed alone governed the injection threshold. Also, at any given CME speed, the high-energy Fe/O spans a large range of values. More importantly, the measured CME speeds in these

events vary by only a factor of ~3. It seems unlikely that a factor of 3 is sufficiently large to drastically alter the injectable seed population. On the other hand, it is believed that shock geometry can easily change the injection threshold by a factor of >10. (See, for example, eqs. [4.59] and [4.60] of Webb et al. 1995.)

Our shock-geometry hypothesis directly addresses one of the most persistent observational puzzles of recent SEP observations—why do so many large gradual SEP events have composition at high-energy that looks like that of flare-accelerated impulsive events? The alternative hypothesis of a direct flare component at high energies is a priori reasonable. But, as we have seen, the observational facts provided by the longitude distribution of enhanced Fe/O events, the absence of spectral discontinuities, and numerous timing studies all pose serious challenges for that hypothesis. However, all of these observations are consistent with the CME-driven shock as the primary accelerator, even at the highest observed energies.

Nevertheless, many critical aspects remain to be worked out, and testing the hypothesis requires additional studies. One particular challenge is to understand in detail events like 2002 August 24, in which Fe/O increases with energy above ~10 MeV nucleon^{-1}. It is possible that this increase reflects an evolution, in which the higher energy particles are produced by a quasi-perpendicular shock that later becomes quasi-parallel and then generates the bulk of the lower-energy particles. In fact, averaging over a changing θ_{Bn}, with the concomitant changes in injection threshold, seed population, and spectral rollovers, can be expected to produce Fe/O that increases with energy (M. A. Lee & A. J. Tylka 2005, in preparation).

Other factors may also come into play. Perhaps also important here is the fact that shocks have only a finite amount of time in which to accelerate the particles to their observed energies. Consequently, it might be expected that the seed particles that start out at higher energies end up at higher energies, at least on average. The rise in Fe/O with energy may therefore actually be tracing out the change in the seed population as it goes from solar-wind–dominated to flare-dominated suprathermals. Theoretical studies are needed to assess whether or not this scenario is plausible.

We have suggested that enhanced high-energy Fe/O indicates a quasi-perpendicular shock, at least while near the Sun. Figure 13 therefore implies that this quasi-perpendicular configuration arises in many events, regardless of the source longitude. At first glance, this notion might be surprising, since it is not what one would expect from the large-scale Parker spiral. However, it must be remembered that the high-energy particles are generally produced when the leading edge of the CME is less than ~15 $R_\odot$ above the photosphere and, in many events, probably substantially lower. For example, the recent timing study of the 2001 April 15 GLE (Bieber et al. 2004) put the peak of the GeV-particle production when the CME was only at ~2–3 $R_\odot$ above the photosphere. At these altitudes, the open solar magnetic field is expected to be predominantly radial. Most CME-driven shocks are therefore likely to have extensive quasi-perpendicular regions at these altitudes. In fact, this behavior is seen in detailed MHD simulations, such as Roussev et al. (2004) (I. Roussev 2004, private communication). Further efforts, in which these MHD simulations are coupled to models of particle acceleration at shocks of evolving obliquity, are needed.

We have only considered energetic protons and ions in this paper. At Earth's bow shock, electrons are more effectively accelerated at quasi-perpendicular configurations (Gosling et al. 1989). This fact suggests that *solar* electrons may carry signatures of *near-Sun* shock geometry. Comparative studies of electrons in the gradual SEP events may therefore provide another means to test our hypothesis. To find the differences it may be necessary to extend the electron observations beyond the ~300 keV maximum energy generally reported by *Wind* and *ACE*.

Similarly, quasi-perpendicular shocks are expected to be more effective at generating type II radio emission (Holman & Pesses 1983; Knock et al. 2003). Imaging shows that the metric type II emission generally originates at coronal altitudes below the leading edge of the CME (Wagner 1982; Gary et al. 1984). Steinolfson (1984) demonstrated that this fact could be understood in terms of shock-drift acceleration of electrons at quasi-perpendicular regions on the flanks of the CME. More recently, Maia et al. (2000) presented Nancy radioheliograph observations of metric type II emission coming from the *leading edges* of CMEs. They noted that this emission is weak and generally goes undetected unless the usual sources of stronger emissions are occulted or otherwise absent. In the low corona, one would generally expect the shock at the CME's leading edge to be quasi-parallel and therefore not particularly effective at accelerating electrons. The relative weakness of the radio emission from the CME's leading edge is therefore perhaps not surprising. Intriguingly, one of the events discussed by Maia et al. (2000) was a major particle event—1998 April 20, whose spectral and composition characteristics (Tylka et al. 2000) are those we would expect for a quasi-parallel shock. Further comparative study of metric type II imaging and SEP characteristics may therefore be instructive. However, it should be noted that such a study may also be inconclusive, in that the radio emission is affected by a number of factors besides shock geometry. Moreover, the conditions implied by the radio emissions may not necessarily apply to Sun-Earth field line.

Finally, our inferences about the near-Sun shock geometry are all indirect, drawn from the energetic particle data alone and without any direct evidence on shock geometry while the CME is near the Sun. Ultimately, the viability of our hypothesis will be addressed by detailed numerical simulations of evolving CME-driven shocks and the resulting particle production as they propagate through realistic models of the corona and interplanetary medium. One would also nevertheless like to find direct solar observations that might bear upon the shock geometry. Nitta et al. (2003) studied the soft X-ray images associated with seven large SEP events from solar cycle 23. Their event sample contained events in which the oxygen spectra showed exponential rollovers and Fe/O at high energies that was suppressed (we would consider these events likely to be quasi-parallel), and other events in which the spectra were power laws without visible rollovers and Fe/O was enhanced at high energies (we would consider these as quasi-perpendicular). In the former case, the ejections occurred over larger spatial regions and with longer timescales involving a slowly expanding pre-eruption phase. On the other hand, events in the second category erupted explosively from a smaller region. Raymond et al. (2003) compared CME-related UV emissions from the events of Figure 1. They also noted that the LASCO images at ~2–6 $R_\odot$ in the 2002 August 24 event "give a strong impression of transverse expansion," while the 2002 April 21 event "has more of the appearance of a cloud of ejected plasma." Further investigation is needed to decide whether observations such as these may provide diagnostics of the near-Sun shock geometry.

This study grew out of discussions at the Living with a Star (LWS) Coordinated Data Analysis Workshop (Gopalswamy

2003), sponsored by NASA in Lanham, Maryland, on 2002 July 22–26. The study also benefitted from further efforts at the 2003 SHINE meeting (sponsored by NSF, NASA, and AFOSR in Maui, HI, on 2003 July 7–11), which highlighted 2002 April 21 and 2002 August 24 as campaign events. We thank the organizers and sponsors of those meetings. We gratefully acknowledge data provided by the *ACE* Science Center, NSSDC, and NOAA. We also gratefully acknowledge the *SOHO* LASCO CME catalog, which is generated and maintained by NASA and The Catholic University of America in cooperation with the Naval Research Laboratory. *SOHO* is a project of international collaboration between ESA and NASA. We thank C. Lopate for Climax neutron data, which is made available through NSF grant ATM 99-12341. We also thank the Bartol Research Institute neutron monitor program, which is supported by NSF under grant ATM 00-00315.

We thank P. R. Boberg, J. Burkepile, A. W. Labrador, J. Mariska, K. Roger Pyle, M. A. Shea, D. F. Smart, and S. Yashiro for additional data. We also thank them and M. Andrews, E. W. Cliver, M. Desai, J. Giacolone, J. R. Jokipii, S. W. Kahler, B. C. Low, R. J. Murphy, N. V. Nitta, M. Reiner, W. K. M. Rice, and G. Share for many helpful comments and discussions. A. J. T. was supported by NASA DPR S13791G and the Office of Naval Research. W. F. D. was supported under NASA DPR S13823G. M. A. L. was supported by NSF grant ATM 00-91527, NASA grant NAG5-11797, and DoD MURI grants to the University of Michigan and the University of California at Berkeley. C. K. N. was supported by NASA grant LWS-784-50-00-08.

REFERENCES

Achterberg, A., & Ball, L. 1994, A&A, 284, 687
Band, D., et al. 1993, ApJ, 413, 281
Barghouty, A. F., & Mewaldt, R. A. 1999, ApJ, 520, L127
———. 2000, in AIP Conf. Proc. 528, Acceleration and Transport of Energetic Particles in the Heliosphere, ed. R. A. Mewaldt et al. (Melville: AIP), 71
Bieber, J. W., Evenson, P., Dröge, W., Pyle, R., Ruffolo, D., Rujiwarodom, M., Toprakai, P., & Khumlumert, T. 2004, ApJ, 601, L103
Bieber, J. W., Matthaeus, W. H., & Salchi, A. 2004, J. Geophys. Res. Lett., 31, 10805
Cane, H. V., Erickson, W. C., & Presage, N. P. 2002, J. Geophys. Res., 107(A10), 1315
Cane, H. V., McGuire, R. E., & von Rosenvinge, T. T. 1986, ApJ, 301, 448
Cane, H. V., Reames, D. V., & von Rosenvinge, T. T. 1988, J. Geophys. Res., 93, 9555
Cane, H.V., von Rosenvinge, T. T., Cohen, C. M. S., & Mewaldt, R. A. 2003, Geophys. Res. Lett., 30(12), 8017
Cliver, E. W., Kahler, S. W., & Reames, D. V. 2004, ApJ, 605, 902
Cohen, C. M. S., et al. 1999, Geophys. Res. Lett. 26, 2697
———. 2003, Adv. Space Res. 32(12), 2649
Cook, W. R., et al. 1993, IEEE Trans. Geosci. Remote Sensing, 31 (3), 557
Debrunner, H., et al. 1997, ApJ, 479, 997
Decker, R. B. 1988, Space Sci. Rev., 48, 195
Desai, M. I., Mason, G. M., Dwyer, J. R., Mazur, J. E., Gold, R. E., Krimigis, S. M., Smith, C. W., & Skoug, R. M. 2003, ApJ, 588, 1149
Desai, M. I., et al. 2004, ApJ, 611, 1156
Dietrich, W. F., & Lopate, C. 1999, Proc. 26th Int. Cosmic Ray Conf. (Salt Lake City), 6, 71
Dietrich, W. F., & Tylka, A. J. 2003, Proc. 28th Int. Cosmic Ray Conf. (Tsukuba), 6, 3291
Eichler, D. 1979, ApJ, 229, 419
Ellison, D., & Ramaty, R. 1985, ApJ, 298, 400
Falcone, A., et al. 2003, ApJ, 588, 557
Forman, M. A., & Webb, G. 1985, in Collisionless Shocks in the Heliosphere: A Tutorial Review, ed. R. G. Stone & B. T. Tsurutani (Geophys. Monogr. 35; Washington: AGU), 91
Garcia-Munoz, M., Mason, G. M., & Simpson, J. A. 1975, ApJ, 201, L145
Gary, D. E., et al. 1984, A&A, 134, 222
Giacalone, J. 2005, ApJ, 624, 765
Giacalone, J., & Jokipii, J. R. 1999, ApJ, 520, 204
Giacalone, J., Jokipii, J. R., & Kóta, J. 1994, J. Geophys. Res., 99, 19, 351
Giacalone, J., Jokipii, J. R., & Mazur, J. E. 2000, ApJ, 532, L75
Gloecker, G., Fisk, L. A., Zurbuchen, T. H., & Schwadron, N. A. 2000, in AIP Conf. Proc. 528, Acceleration and Transport of Energetic Particles in the Heliosphere, ed. R. A. Mewaldt et al. (Melville: AIP), 221
Gloeckler, G., & Geiss, J. 1998, Space Sci. Rev., 84, 275
Gold, R. E., et al. 1998, Space Sci. Rev., 86, 541
Gopalswamy, N. 2003, Geophys. Res. Lett., 30, 8013
Gosling, J. T., Thomsen, M. F., Bame, S. J., & Russell, C. T. 1989, J. Geophys. Res., 94, 10011
Haggerty, D. K., & Roelof, E. C. 2002, ApJ, 579, 841
Holman, G. D., & Pesses, M. E. 1983, ApJ, 267, 837
Jokipii, J. R. 1987, ApJ, 313, 842
Jones, F. C., Baring, M. G., & Ellison, D. C. 1993, Proc. 23rd Int. Cosmic Ray Conf. (Calgary), 2, 243
Jones, F. C., & Ellison, D. 1991, Space Sci. Rev. 58, 259
Kahler, S. W. 1994, ApJ, 428, 837
———. 1999, Proc. 26th Int. Cosmic Ray Conf. (Salt Lake City), 6, 248
Kahler, S. W., Aurass, H., Mann, G., & Klassen, A. 2005, in IAU Symp. 226, Stellar and Coronal Mass Ejections, ed. K. P. Dere, J. Wang, & Y. Yan (Cambridge: Cambridge Univ. Press), in press
Knock, S. A., Cairns, I. H., Robinson, P. A., & Kuncic, Z. 2003, J. Geophys. Res., 108(A3), 1126
Krucker, S., et al. 1999, ApJ, 519, 864
Labrador, A. W., Leske, R. A., Mewaldt, R. A., Stone, E. C., & von Rosenvinge, T. T. 2003, Proc. 28th Int. Cosmic Ray Conf. (Tsukuba), 6, 3269
Laivola, J., Torsti, J., & Kocharov, K. 2003, Proc. 28th Int. Cosmic Ray Conf. (Tsukuba), 6, 3233
Lee, M. A. 1982, J. Geophys. Res., 87, 5063
———. 1997, in Coronal Mass Ejections, ed. N. Crooker, J. A. Jocelyn, & J. Feynman (Geophys. Monogr. 99; New York: AGU), 277
———. 2000, in AIP Conf. Proc. 528, Acceleration and Transport of Energetic Particles in the Heliosphere, ed. R. A. Mewaldt et al. (Melville: AIP), 3
———. 2005, ApJ, in press
Leske, R. A., Cummings, J. R., Mewaldt, R. A., Stone, E. C., & von Rosenvinge, T. T. 1995, ApJ, 452, L149
Leske, R. A., Mewaldt, R. A., Cummings, A. C., Stone, E. C., & von Rosenvinge, T. T. 2001, in AIP Conf. Proc. 598, Solar and Galactic Composition, ed. R. F. Wimmer-Schweingruber (Melville: AIP), 171
Leske, R. A., Wiedenbeck, M. E., Cohen, C. M. S., Mewaldt, R. A., Cummings, A. C., Stone, E. C., & von Rosenvinge, T. T. 2003, Proc. 28th Int. Cosmic Ray Conf. (Tsukuba), 6, 3253
Leske, R. A., et al. 2000, in AIP Conf. Proc. 528, Acceleration and Transport of Energetic Particles in the Heliosphere, ed. R. A. Mewaldt et al. (Melville: AIP), 293
Li, G., Zank, G. P., & Rice, W. K. M. 2003, J. Geophys. Res., 108(A2), 1082
Lin, R. P., Potter, D. W., Gurnett, D. A., & Scarf, F. L. 1981, ApJ, 251, 364
Lockwood, J. A., Debrunner, H., Flueckiger, E. O., & Ryan, J. M. 2002, Sol. Phys., 208, 113
Luhn, A., Klecker, B., Hovestadt, D., & Möbius, E. 1987, ApJ, 317, 951
Maia, D., Pick, M., Vourlidas, A., & Howard, R. 2000, ApJ, 528, L49
Mason, G. M., Mazur, J. E., & Dwyer, J. R. 1999a, ApJ, 525, L133
Mason, G. M., et al. 1998, Space Sci. Rev., 86, 409
———. 1999b, Geophys. Res. Lett., 26, 141
———. 2002, ApJ, 574, 1039
———. 2004, ApJ, 606, 555
Mazur, J. E., Mason, G. M., Dwyer, J. R., Giacolone, J., Jokipii, J. R., & Stone, E. C. 2000, ApJ, 532, L79
Mazur, J. E., Mason, G. M., Klecker, B., & McGuire, R. E. 1992, ApJ, 401, 398
Mewaldt, R. A., et al. 2003a, Proc. 28th Int. Cosmic Ray Conf. (Tsukuba), 6, 3229
———. 2003b, Proc. 28th Int. Cosmic Ray Conf. (Tsukuba), 6, 3313
Meziane, K., Hull, A. J., Hamza, A. M., & Lin, R. P. 2002, J. Geophys. Res., 107, 1243
Möbius, E., et al. 1998, Space Sci. Rev., 86, 449
Ng, C. K., Reames, D. V., & Tylka, A. J. 1999, Geophys. Res. Lett., 26, 2145
———. 2003, ApJ, 591, 461
Nitta, N., Cliver, E. W., & Tylka, A. J. 2003, ApJ, 586, L103
Ostrowski, M. 1988, MNRAS, 233, 257
Poirier, J., & D'Andrea, C. 2002, J. Geophys. Res., 107(A11), 1376
Raymond, J. C., et al. 2003, ApJ, 597, 1106
Reames, D. V. 1995, Adv. Space Res., 15(7), 41
———. 1999, Space Sci. Rev., 90, 413
———. 2000, ApJ, 540, L111
———. 2002, ApJ, 571, L63

Reames, D. V., Barbier, L. M., & Ng, C. K. 1996, ApJ, 466, 473
Reames, D. V., & MacDonald, F. B. 2003, ApJ, 586, L99
Reames, D. V., & Ng, C. K. 2004, ApJ, 610, 510
Reames, D. V., Ng, C. K., & Tylka, A. J. 1999, Geophys. Res. Lett., 26, 3588
Reames, D. V., von Rosenvinge, T. T., & Lin, R. P. 1985, ApJ, 292, 716
Rice, W. K. M., Zank, G. P., & Li, G. 2003, J. Geophys. Res., 108(A10), 1369
Richardson, I. G., Reames, D. V., Wenzel, K.-P., & Rodrigeuz-Pacheco, J. 1990, ApJ, 363, L9
Roussev, I. I., Sokolov, I. V., Forbes, T. G., Gombosi, T. I., Lee, M. A., & Sakai, J. I. 2004, ApJ, 605, L73
Ryan, J. M., Lockwood, J. A., & Debrunner, H. 2000, Space Sci. Rev., 93, 35
Shea, M. A., & Smart, D. F. 1993, in Solar Proton Events: History, Statistics, and Predictions, ed. J. Hruska et al. (Boulder: NOAA), 48
Simnett, G. M., Roelof, E. C., & Haggerty, D. K. 2002, ApJ, 579, 854
Steinolfson, R. S. 1984, Sol. Phys., 94, 193
Stone, E. C., et al. 1998a, Space Sci. Rev., 86, 357
———. 1998b, Space Sci. Rev., 86, 285
Torsti, J., Laivola, J., & Kocharov, L. 2003, A&A, 408, L1
Tsurutani, B. T., & Lin, R. P. 1985, J. Geophys. Res., 90, 1
Tylka, A. J. 2001, J. Geophys. Res., 106, 25333
Tylka, A. J., Boberg, P. R., McGuire, R. E., Ng, C. K., & Reames, D. V. 2000, in AIP Conf. Proc. 528, Acceleration and Transport of Energetic Particles in the Heliosphere, ed. R. A. Mewaldt et al. (Melville: AIP), 147
Tylka, A. J., & Dietrich, W. F. 1999, Radiat. Meas., 30 (3), 345
Tylka, A. J., et al. 1995, ApJ, 444, L109
———. 2001, ApJ, 558, L59
———. 2002, ApJ, 581, L119
———. 2003, Proc. 28th Int. Cosmic Ray Conf. (Tsukuba), 6, 3305
van Nes, P., Reihnard, R., Sanderson, T. R., Wenzel, K.-P., & Zwickl, R. D. 1984, J. Geophys. Res., 89, 2122
von Rosenvinge, T. T., et al. 1995, Space Sci. Rev., 71, 155
———. 2001, in AIP Conf. Proc. 598, Solar and Galactic Composition, ed. R. F. Wimmer-Schweingruber (Melville: AIP), 343
Wagner, W. J. 1982, Adv. Space Res., 2, 203
Webb, G. M., Zank, G. P., Ko, C. M., & Donohue, D. J. 1995, ApJ, 453, 178
Wiedenbeck, M. E., et al. 2000, in AIP Conf. Proc. 528, Acceleration and Transport of Energetic Particles in the Heliosphere, ed. R. A. Mewaldt et al. (Melville: AIP), 107
———. 2003, in AIP Conf. Proc. 679, Solar Wind 10, ed. M. Velli, R. Bruno, & F. Malara (Melville: AIP), 652
Yoshimori, M., Suga, K., Nakayama, S., Takeda, H., Ogawa, H., Murphy, R. J., & Share, G. H. 2002, Adv. Space. Res. 30(3), 629
Zank, G. P., Li, G., Florinski, V., Matthaeus, W. H., Webb, G. M., & le Roux, J. A. 2004, J. Geophys. Res. 109(A0), 4107
Zank, G. P., Rice, W. K. M., & Wu, C. C. 2000, J. Geophys. Res., 105, 25, 079